DETECTING CLINICAL BIOMARKERS USING DIFFUSION TENSOR IMAGING

by

TEJASVI GUNDAPUNEEDI

Presented to the Faculty of the Graduate School of

The University of Texas at Arlington in Partial Fulfillment

of the Requirements

for the Degree of

MASTER OF SCIENCE IN BIOMEDICAL ENGINEERING

THE UNIVERSITY OF TEXAS AT ARLINGTON

May 2012

ACKNOWLEDGEMENTS

It gives me immense pleasure and joy to thank all the people who supported and assisted me throughout the last year.

First, and foremost, I would like to thank my advisor Dr. Hao Huang for giving me an opportunity to be a part of his team. His constant encouragement and guidance in the past year helped me gain a lot of knowledge in the field of brain research. He is very patient in explaining and answering all my concerns.

I would also like to thank Dr. Mario I. Romero-Ortega and Dr.Hanzhang Lu who agreed to be on my committee and for providing feedback on my research.

I am also grateful to the administrative staff of the departments of biomedical engineering (BME at UTA – UTSW) and Advanced Radiological Sciences (UTSW) for assisting me in many different ways.

Lastly, and most importantly, I wish to thank my family for their unconditional love and support during all my endeavors. Anything and everything I have accomplished so far, is due to their support.

March 21, 2012

ABSTRACT

DETECTING CLINICAL BIOMARKERS USING DIFFUSION TENSOR IMAGING

Tejasvi Gundapuneedi, M.S

The University of Texas at Arlington, 2012

Supervising Professor: Hao Huang.

Diffusion tensor imaging (DTI), a modality of MRI that measures water diffusion properties noninvasively, is highly sensitive to subtle structural changes of white matter. It provides a unique and noninvasive method for delineating *in-vivo* architecture of human brain white matter. Four metrics derived from DTI, fractional anisotropy (FA), mean diffusivity (MD), axial diffusivity (AxD) and radial diffusivity (RD), have been widely used to quantitatively characterize the white matter disruption in mental disorders and degenerative diseases. An atlas-based approach incorporating a digital white matter atlas and registration and skeletonisation functions of tract-based spatial statistics (TBSS) has been developed recently. This approach effectively delineates the white matter disruption at both voxel level and tract level. More importantly, the information on disruption of the functional tracts has clinical significance. In our studies, we have applied this approach to two important clinical groups, maltreated children and elderly subjects with amnestic mild cognitive impairment (aMCI). Maltreated children are more vulnerable than normal group to develop mental disorders. The early traits of white matter structural abnormality in this could be found in our study. aMCI involves the onset and evolution of cognitive impairment. The elderly subjects with aMCI have higher risk of later developing dementia, including Alzheimer's disease (AD). In our study, the integrity changes of limbic system tracts, which are severely damaged in AD, for aMCI subjects,

were revealed. These limbic tract changes could serve as the potential early white matter biomarker for AD.

TABLE OF CONTENTS

LIST OF ILLUSTRATIONS

Figure Page

LIST OF TABLES

LIST OF ABBREVIATIONS

MRI	Magnetic Resonance Imaging
NMR	Nuclear Magnetic Resonance
DTI	Diffusion Tensor Imaging
DWI	Diffusion Weighted Imaging
AD	Alzheimer's
FA	Fractional Anisotropy
AxD	Axial Diffusivity
RD	Radial Diffusivity
MD	Mean Diffusivity
EPI	Echo Planar Imaging
TE	Echo Time
TR	Repetition Time
SNR	Signal to Noise Ratio
FOV	Field of View
TBSS	Tract Based Spatial Statistics
CNS	Central Nervous System
CST	Corticospinal Tract
ATR	Anterior Thalamic Radiation
STR	Superior Thalamic Radiation
PTR	Posterior Thalamic Radiation
SLF	Superior Longitudinal Fasciculus
ILF	Inferior Longitudinal Fasciculs
IFO	Inferior Fronto-occipital Fasciculus

UF	Uncinate Fasciculus
CG	Cingiulum
FX	Fornix
ST	Stria Terminalis
CC	Corpus Callosum
Fmajor	Forceps Major
Fminor	Forceps Minor
SCR	Superior Corona Radiata

CHAPTER 1

INTRODUCTION

1.1 Theoretical Background of Diffusion Tensor Imaging

Magnetic Resonance Imaging (MRI) is a non-invasive, non-ionizing imaging technique based on the principles of Nuclear Magnetic Resonance (NMR) (Bloch, 1946; Purcell et al., 1946). Diffusion tensor imaging (DTI) is another modality of MRI, which is also based on the principles of NMR. In 1965, the diffusion constant of water molecules was first measured by Drs. Stejskal and Tanner using NMR and magnetic field gradients. In 1979, the anisotropic diffusion of frog muscle was measured by Dr.Tanner. In 1980's Le Bihan enabled the acquisition of diffusion weighted imaging (DWI) with spatially varying measurements of the diffusion rate of water. Basser later introduced the diffusion tensor formalism to characterize the anisotropic diffusion found in white matter structures(Basser, Mattiello, & LeBihan, 1994). The development of DWI and diffusion tensor imaging (DTI) has enabled detailed investigation of white matter fiber bundles by mapping the anisotropic diffusion of water generated by axon fiber bundles.

1.2 Basic Principles of Diffusion Tensor Imaging

Molecular diffusion refers to the random translational motion of molecules also called Brownian motion that results from the thermal energy carried by these molecules, a physical process that was well characterized by Einstein. In a free medium, during a given time interval, molecular displacements obey a three dimensional Gaussian distribution, that is statistically well described by diffusion coefficient (D), as shown in figure 1.1. This coefficient, D depends only on the size (mass) of molecules, the temperature and the nature (viscosity) of the medium.

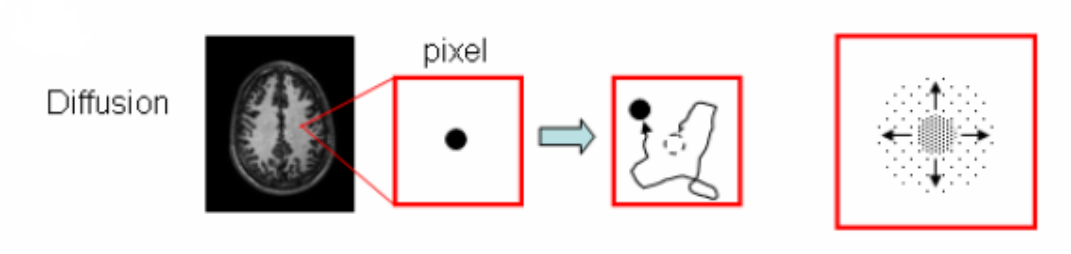

Figure 1.1: The diffusion of water molecule.

To measure the diffusion coefficient using MRI, magnetic field gradients are required. This is how the gradients help in the measurement of diffusion coefficient. After the first excitation pulse is applied, all the protons in the sample release the signal at the same frequency. Once the first gradient is applied protons at different locations experience different magnetic field and by the end of gradient application, the phases of signal among protons are not identical. If a second gradient is applied with reverse polarity for the same amount of time as the first, the protons should regain the phase. However, perfect refocusing happens only when the water molecules are still in between the application of two gradients. The water molecules diffuse randomly which makes the perfect rephasing impossible and this causes a loss in the signal. The diffusion of water molecules can be detected by the loss of signal intensity after the application of second gradient. The signal intensity(S) is dependent on four parameters, diffusion coefficient (D), Gradient strength (G), length of gradient (δ) and time between the applications of the two gradients (Δ).

$$\mathbf{S = f(D, G, \Delta, \delta)}$$

Of the four parameters on which the signal intensity depends, the diffusion coefficient is the only unknown parameter. We can measure the signal intensity from the experiment and calculate the diffusion coefficient (D). To find the amount of signal lost we need to measure at least two signals, one without applying any gradients and the other applying gradients. If we consider S_0 as signal intensity without gradients and S as signal intensity with gradients, the equation to calculate diffusion coefficient D is,

$$S = S_0 e^{-\gamma^2 G^2 \delta^2 D(\Delta - \frac{\delta}{3})} \text{ ..... Eq: 1.2.1}$$

γ is the gyromagnetic ratio and its value is 2.765 x 10^8/s,T for a proton. For detailed explanation of the equation 1.2.1 refer to Introduction to Diffusion Tensor Imaging by Mori.

1.3 From Diffusion Signal to Diffusion Tensor

Diffusion sometimes has directionality. When water diffuses freely it assumes the shape of a sphere and it is called isotropic diffusion. If there is any hindrance, then water does not diffuse equally in all directions. This is called anisotropic diffusion. Both isotropic and anisotropic diffusion are shown visually in figure 1.2. In case of isotropic diffusion, the diffusion constant (D), is enough to describe the diffusion. The diffusion constant is related to the diameter of the sphere and a sphere needs only one parameter to be uniquely determined. In case of anisotropic diffusion, the diffusion takes the shape of an ellipsoid and single parameter will not be sufficient to describe the process of diffusion. This phenomenon is shown in figure 1.3.

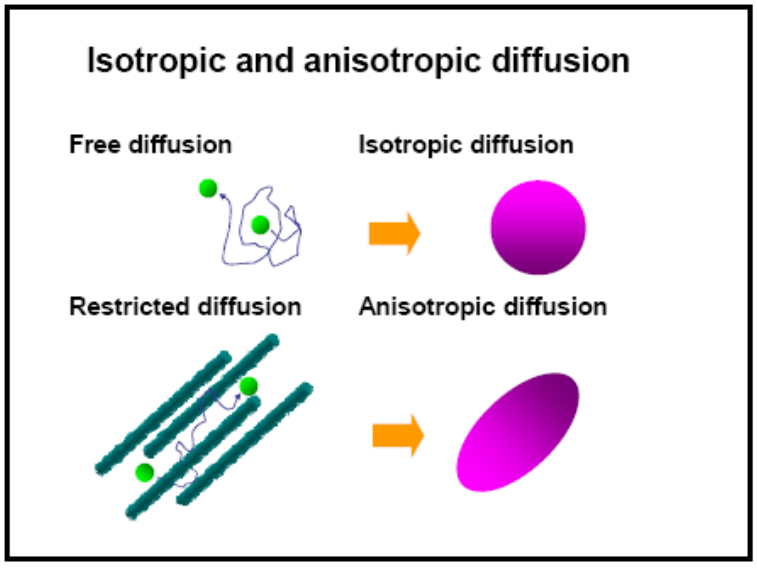

Figure 1.2: Illustrative representation of isotropic and anisotropic diffusion.

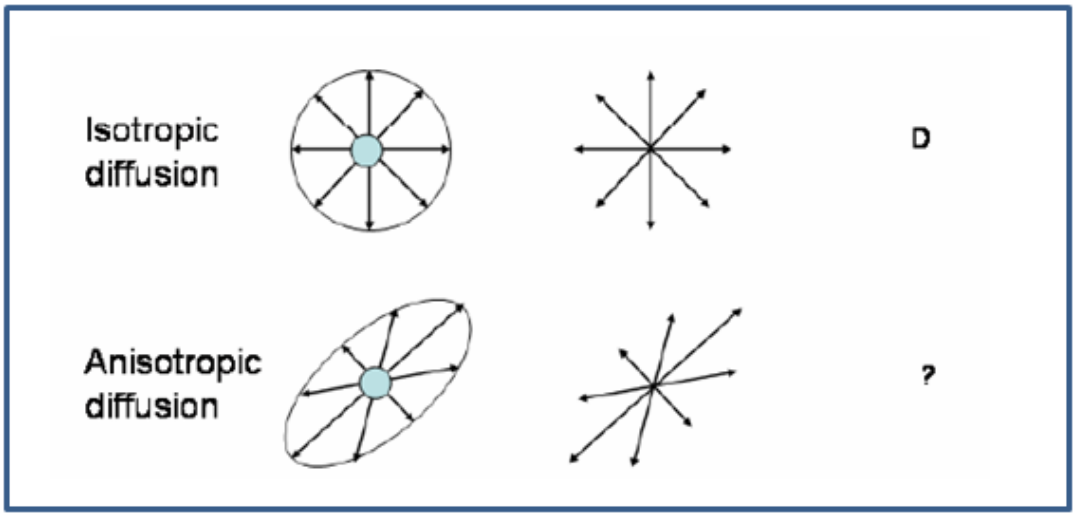

Figure 1.3: Comparison between isotropic and anisotropic diffusion

To characterize the anisotropic diffusion, at least six parameters are needed to define an ellipsoid. We need three lengths for the longest, shortest and the middle axes that are perpendicular to each other. The three lengths are usually called the Eigen values, λ_1, λ_2, λ_3. To describe the orientation of the principle axes of the ellipsoid we can use three vectors v_1, v_2, and v_3, referred to as Eigen vectors. Figure 1.4 describes how the Eigen values and vectors describe an ellipsoid.

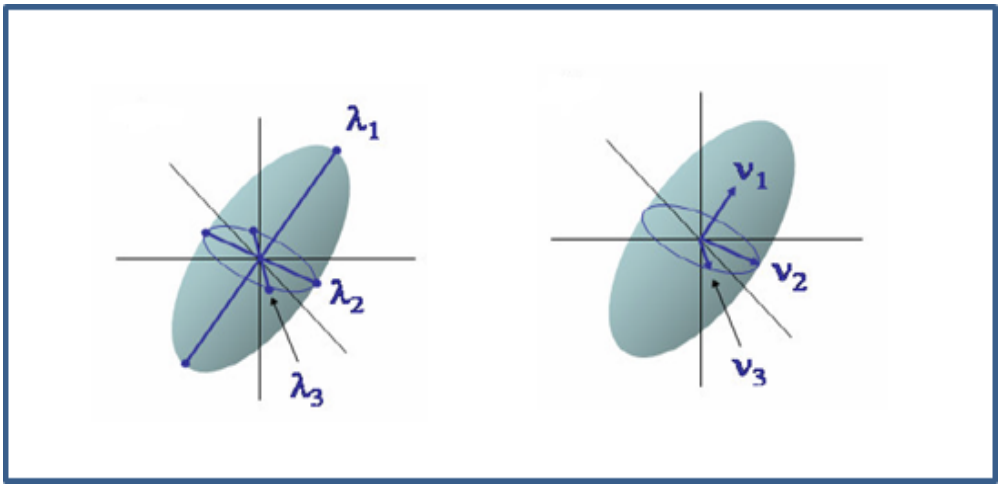

Figure 1.4: Parameters needed to define a 3D ellipsoid

The anisotropic diffusion is of great interest because it carries much information about underlying anatomical architecture of living tissues. Whenever there is ordered structures such as axonal tracts in nervous tissues or protein filaments in muscle, water tends to diffuse along such structures. If we can determine the way water diffuses, we can obtain precious information about the object.

From a series of diffusion weighted images, employing diffusion sensitization in six independent directions, a diffusion tensor can be calculated in each voxel (Basser et al. 1994*a*). More than six measurements can be used to more accurately define the ellipsoid under the existence of measurement errors. Usually measurements are made along 30 directions to fit the tensor (Jones, Horsfield, & Simmons, 1999). To determine the six parameters, λ_1, λ_2, λ_3, v_1, v_2, and v_3 that describe the diffusion ellipsoid a 3x3 tensor, called diffusion tensor, $\overline{\overline{\boldsymbol{D}}}$, is used which is related to the six parameters by a process called diagonalization.

$$\overline{\overline{\boldsymbol{D}}} = \begin{bmatrix} \boldsymbol{D_{xx}} & \boldsymbol{D_{xy}} & \boldsymbol{D_{xz}} \\ \boldsymbol{D_{yx}} & \boldsymbol{D_{yy}} & \boldsymbol{D_{yz}} \\ \boldsymbol{D_{xz}} & \boldsymbol{D_{yz}} & \boldsymbol{D_{zz}} \end{bmatrix} \xrightarrow{\boldsymbol{Diagonalization}} \lambda_1, \lambda_2, \lambda_3, v_1, v_2, v_3$$

The eigenvalues and eigenvectors of this tensor provide information about local tissue anisotropy. The eigenvector belonging to the largest Eigen value of the diffusion tensor is assumed to coincide with the myelinated fiber direction in brain white matter. (Pierpaoli & Basser, 1996)

Once the Eigen values and vectors are computed from the tensor using these values we can compute DTI metrics, fractional anisotropy (FA), axial diffusivity (AxD), radial diffusivity (RD) and mean diffusivity (MD). Axial diffusivity reflects the diffusion coefficient along the direction of maximal apparent diffusion, AxD = λ_1. Radial diffusivity reflects the average diffusion coefficients along the two perpendicular directions, RD = $((\lambda_2 + \lambda_3)/2)$. Mean diffusivity is a scalar measure of the total amount of diffusion within a voxel and is computed as an average of all three eigenvalues of the diffusion tensor, MD = $((\lambda 1 + \lambda 2 + \lambda_3)/3)$. Fractional anisotropy is

computed as a weighted average of the three eigenvalues of the diffusion tensor in order to represent the fraction of the tensor defined by anisotropic diffusion,

$$FA = \frac{\sqrt{(\lambda_1 - \lambda_2)^2 + (\lambda_2 - \lambda_3)^2 + (\lambda_1 - \lambda_3)^2}}{\sqrt{2(\lambda_1{}^2 + \lambda_2{}^2 + \lambda_3{}^2)}}$$

The FA value ranges from 0 to 1. In the case of isotropic diffusion FA = 0.

1.4 Overview of White Matter Anatomy

The central nervous system (CNS) which includes the brain and spinal cord is responsible for cognitive thought, sensory information processing, homeostatic regulation and control of motor function in human body. The principle information processing cells of CNS are called neurons, which have cell bodies, dendrites and axons, and supporting cells of neurons called glial cells shown in Figure 1.5.

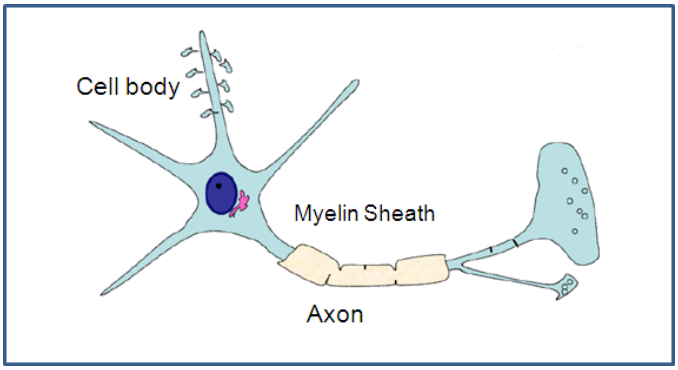

Figure 1.5: The structure of neuron

Estimates for the number of neurons in the human brain range from 80 to 120 billion (Azevedo et al., 2009). The areas of the CNS that are mainly composed of cell bodies is called the gray matter and areas that include axon bundles is called white matter. The gray matter is located around the outside of the brain in the highly convoluted cortex (with “ridges” called gyri and “valleys” called sulci) and in internal brain structures such as the basal ganglia and thalamus.

The white matter contains the axonal pathways that interconnect the brain (bundles of axons traveling together and are called white matter fiber tracts). The brain has two hemispheres, the right and left, whose functions are complimentary. The brain is further divided into five lobes in each hemisphere, the frontal, parietal, temporal, occipital, and limbic lobes as shown in Figure 1.6 with unique functions for each lobe.

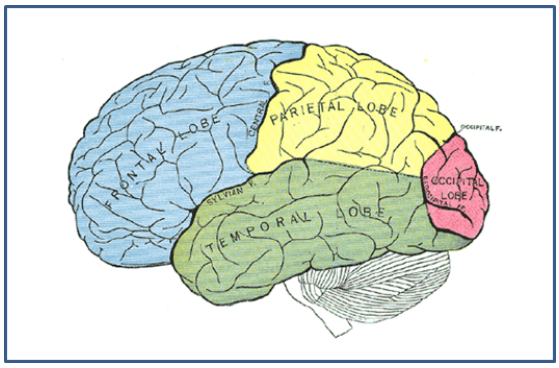

Figure 1.6: The four lobes of the brain, Frontal lobe (blue), parietal lobe (yellow), temporal lobe (green) and occipital lobe (pink).

The lobes of the brain are interconnected by the white matter fiber tracts, which are classified into five functional categories, tracts in brainstem, projection fibers, association fibers, limbic fibers, and commissural fibers (Wakana, Jiang, Nagae-Poetscher, van Zijl, & Mori, 2004).

Projection fibers are white matter fibers that connect the cortex to the spinal cord, brainstem and thalamus. Projection fibers include the corticospinal tract (CST), anterior thalamic radiation (ATR), superior thalamic radiation (STR) and posterior thalamic radiation (PTR). The projection fibers are shown in figure 1.7. The figure 1.7 is from Wakana et al., 2004.

The association fibers are fibers that connect different regions of cortex which includes long range, short range and cortical U fibers. The association tracts include superior longitudinal fasciculus (SLF), inferior longitudinal fasciculus (ILF), inferior fronto-occipital fasciculus (IFO), and uncinate fasciculus (UF) as depicted in figure 1.8. The figure 1.8 is from Wakana et al., 2004.

The limbic fiber system includes cingulum (CG), fornix (FX), and stria terminalis(ST), shown in figure 1.9. The figure 1.9 is from Wakana et al., 2004.

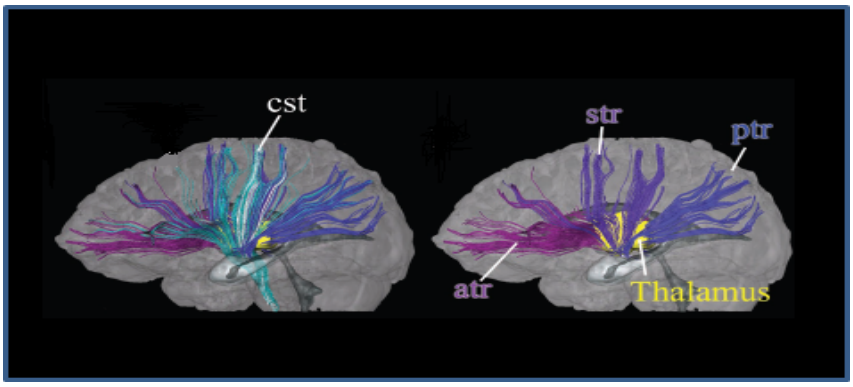

Figure 1.7: Projection fibers, cortiocospinal tract =cst (white), anterior thalamic radiation= atr (bright purple), superior thalamic radiation=str (purple) and posterior thalamic radiation= ptr (dark blue) on a coronal slice.

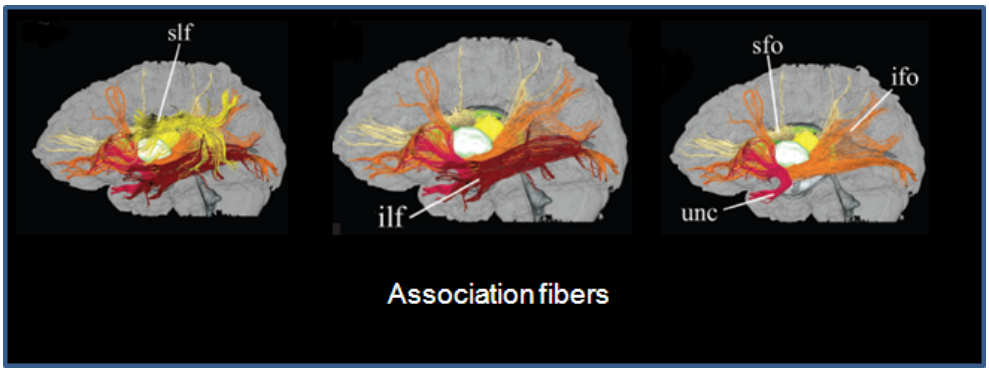

Figure 1.8: Association fibers, superior longitudinal fasciculus = slf (yellow), inferior longitudinal fasciculus = ilf (brown), inferior fronto-occipital fasciculus= ifo (orange), superior fronto-occipital fasciculus =sfo (beige) and uncinate fasciculus= unc (red). Figure from (Wakana et al., 2004)

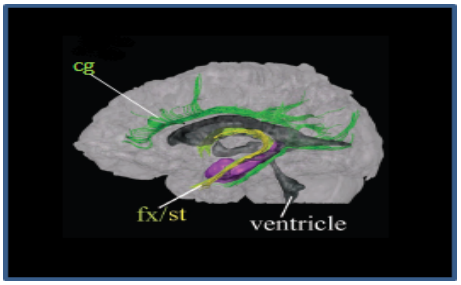

Figure 1.9: The limbic fibers, cingulum= cg(green), fornix=fx(light green) and stria terminalis=st(yellow).

The callosal fibers connect the opposite hemisphere, which includes the corpus callosum (CC) and its extensions forceps major (Fmajor) and forceps minor (Fminor), shown in figure 1.10. The figure 1.10 is from Wakana et al., 2004.

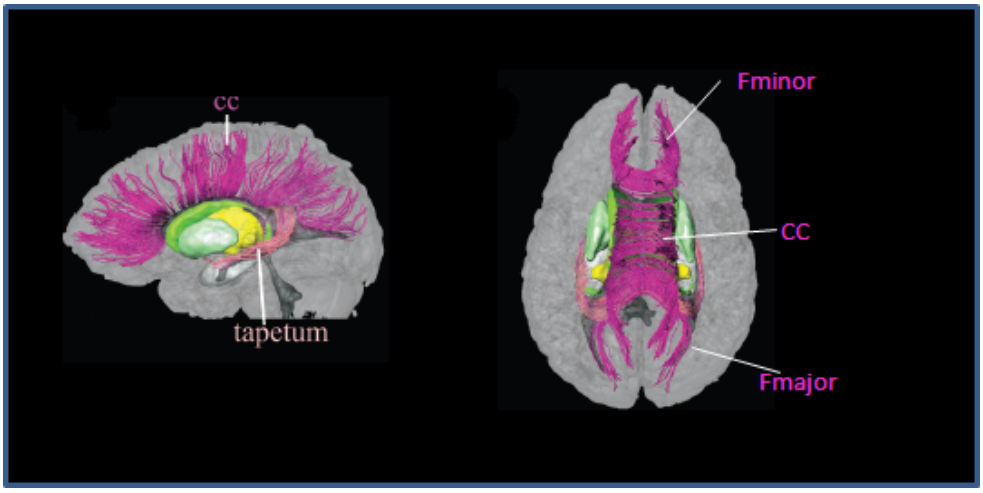

Figure 1.10: The callosal fibers, Corpus callosum = cc (pink), the extension from genu Forceps minor= Fminor and extension from splenium Forceps major = Fmajor. The left figure is the left sagittal view and the right is the axial view..

1.5 Aim of the study

The aim of this study is to use diffusion tensor imaging data and apply techniques like voxel-wise analysis, cluster analysis and tract-level analysis on the data to identify white matter structure abnormalities. To better understand the nature of white matter disruption, data analysis is performed on four DTI metrics, fractional anisotropy (FA), mean diffusivity (MD), axial diffusivity (AxD) and radial diffusivity (RD). In this study, the techniques are applied to two study groups, childhood maltreatment and mild cognitive impairment and the disruptions in white matter tracts are identified.

1.6 Background of clinical groups under study

1.6.1 Childhood Maltreatment

Childhood maltreatment includes both abuse and neglect that harms a child. Several studies conducted on children exposed to maltreatment have seen numerous negative outcomes such as delinquency, pregnancy, alcohol and drug abuse, school failure, and

emotional and mental health problems in the adulthood. Adolescence is a crucial developmental stage marked by a confluence of physical, biological, psychological and social challenges ((Blakemore, Burnett, & Dahl, 2010; Sisk & Foster, 2004; Somerville, Jones, & Casey, 2010; Wahlstrom, White, & Luciana, 2010). There are significant physical maturational changes (e.g., the onset of puberty), social-cognitive advances (e.g., ability for more abstract-thinking and generalizations across situations and time), interpersonal transitions (e.g., changes in social roles in family and peer relationships), and social-contextual changes (e.g., school transitions). Although these maturational transitions offer tremendous opportunities for youth, because the developing brain regions underlying emotional, cognitive and behavioral systems mature at different rates, this developmental period also is marked by heightened vulnerability to psychopathology ((Brenhouse & Andersen, 2011; Ernst & Korelitz, 2009; Paus, Keshavan, & Giedd, 2008; Somerville et al., 2010; Wahlstrom et al., 2010). Specifically, adolescents with a history of childhood maltreatment constitute a high-risk group for the development of psychopathology. Stress endured in early life, during a time of neural plasticity, may induce cognitive and other neural changes which may predispose individuals to a variety of emotional behavioral disorders, mood and substance use disorders among others (Andersen & Teicher, 2008; De Bellis, 2002; Enoch, 2011; Heim & Binder, 2012). For example, several preclinical and clinical investigations have shown an association between early-life stress and alterations in gray and white matter in pediatric and adult samples (McCrory, De Brito, & Viding, 2010; Teicher, Tomoda, & Andersen, 2006). Neuroimaging studies conducted on the maltreated children have shown structural changes in the brain anatomy (van Harmelen et al., 2010; Kaufman & Charney, 2001). However, it is not clear whether these alterations, in fact, increase vulnerability to psychopathology. In the current study, we examined whether healthy adolescents who had no prior history of psychopathology but who had been exposed to maltreatment during childhood show alterations in white matter tracts and whether these alterations are associated with an increased likelihood of developing mood and/or substance

use disorders during prospective follow-up. So, using the current study we can identify changes in the white matter structures that can be used as clinical biomarkers even before the onset of illness and appropriate preventive treatment can be provided for the maltreated children.

1.6.2 Amnestic Mild Cognitive Impairment (aMCI)

Mild cognitive impairment (MCI) is a condition characterized by a memory deficit, but not dementia. It is further classified into subtypes amnestic MCI (aMCI) and non-amnestic MCI (naMCI) based on the presence or absence of memory impairment (Petersen, 2004). naMCI is characterized by non-memory cognitive dysfunction. The aMCI is characterized by memory loss, but the cognitive functions and activities of daily life remain normal. aMCI patients are particularly associated with an increased risk of developing Alzheimer's disease (AD) (Cui et al., 2012).Studies indicate that there is a 10–15% annual incidence of conversion of aMCI to AD (Petersen et al., 2001).Patients with AD has severe memory and cognitive impairment which interfere with the daily life. Several DTI studies conducted on AD patients have observed white matter structural changes. (Acosta-Cabronero, Williams, Pengas, & Nestor, 2010; Bosch et al., 2012; Gold, Johnson, Powell, & Smith, 2012; Huang et al., 2011), White matter disruption was observed in the limbic fibers, association fibers, commissural and projection fibers in the AD patients. Studies conducted on AD have helped to understand the neurodegenration associated with the disease, but clinical intervention on the AD patients are disappointing (Wang et al., 2012). Neuroimage studies on aMCI patients who are more vulnerable to developing AD, and identifying imaging biomarkers can give us a better understanding of the progression of the disease and also provide an opportunity to slow down the progression or totally avoid the development of AD. In the current cross-sectional study we studied white matter changes in 23 aMCI patients comparing to the 19 healthy age matched controls. Local white matter disruptions are seen in limbic tracts (Cingulum, and Fornix) and also in association fibers (SLF and UNC/IFO), where the FA is decreased in aMCI patients compared to healthy controls. The results also indicated that the disruption is only in particular regions of the tract and not the

entire tract. Similar changes in the limbic and association fiber tracts are seen in the AD studies but there is significant difference in FA in the entire tract. The results obtained in the current study indicate that we can use the local white matter disruption observed in the limbic tracts as clinical biomarkers to detect the early onset of AD in the aMCI patients.

1.7 Organization of Thesis

The content of this thesis is presented as follows. Chapter 2 has details about the subject demographics and the methods employed to identify the white matter structure abnormalities. Chapter 3 has all the results that are obtained for the childhood maltreatment study and aMCI study. Chapter 4 has discussion about the results and Chapter 5 concludes the study.

CHAPTER 2

MATERIALS AND METHODS

2.1 Participants

The subject demographics of the two clinical groups, childhood maltreatment and aMCI under study are as follows:

2.1.1 Childhood Maltreatment study

For this study a total of 32 adolescent subjects who do not have any psychiatric illness were recruited with approval from local Institutional Review Board. All the participants were medically healthy and free from alcohol or illicit drug use, as determined by physical examination, full chemistry panel, thyroid function tests, electrocardiogram and urine drug screens. The Drug use Screening Inventory (DUSI), which is a self-report instrument designed to assess the severity of alcohol/drug abuse and related psychiatric and psychological problems was used to assess substance-related problems. A rating above 0.3 is considered as substance-related problem.19 of these subjects were exposed to childhood maltreatment, which includes physical abuse, sexual abuse and/ or witnessed domestic violence lasting 6 months or longer, prior to the age 10. Information on early-life adversity was obtained with a semi-structured interview, the Childhood Adversity Interview. Adolescent participant and parent were interviewed separately. Information was obtained on seven subtypes of childhood adversity that persisted for 6 months or longer (including separation/loss of caretaker, life-threatening illness/injury in the self or others, physical neglect, emotional abuse/assault, physical abuse/assault, witnessing domestic violence, and sexual abuse/assault) that occurred prior to age 10 years. The adverse impact (1 = no adversity, and 5 = most severe form of adversity)

was based on summaries of events, circumstances and their contexts. Information from both informants was combined for the summary ratings. An early-life adversity score was tabulated from the sum of ratings from the seven adversity domains. The other 13 subjects are used as controls and have no history of maltreatment or family history of a psychiatric disorder. Symptoms of psychiatric disorders were assessed using the Schedule for Affective Disorders and Schizophrenia for School-Age Children - the Present and Lifetime Version (K-SADS-PL). The Family History-Research Diagnostic Criteria (FH-RDC), a semi-structured interview, was used for the evaluation of psychiatric disorders in family members (Andreasen, Endicott, Spitzer, & Winokur, 1977). The subjects' demographics are outlined in table 2.1. The data is presented as means and standard deviations or as raw numbers

Table 2.1: Subject demographics for childhood maltreatment study

	Control (n=13)	**Maltreated (n=19)**
Age (years)	16.00± 2.74	15.89 ± 2.79
Gender (male/female)	6/7	5/14
Ethnicity(Caucasian /Non-Caucasian)	9/4	12/7
Drug Use Screening Inventory	0.08±0.06	0.13±0.39
Childhood Adversity	7.62 $\pm$ 0.65	14.70 $\pm$ 3.98

2.1.2 aMCI study

From a longitudinal study on amnestic mild cognitive impairment a total of 42 subjects are used for the current cross-sectional study. 23 of the 42 subjects are diagnosed as aMCI patients. The remaining 19 are age and education matched normal subjects with no memory or cognitive decline. Consortium to Establish a Registry for Alzheimer's disease (CERAD) and

Mini-Mental State Examination (MMSE) scores were also obtained from the subjects. Subjects' demographics are outlined in table 2.2. The data is presented as means and standard deviations or as raw numbers.

Table 2.2: Subject demographics for amnestic mild cognitive impairment study

	Control (n=19)	**aMCI (n=23)**
Age (years)	67.47+/-6.99	66.78+/-6.63
Gender (male/female)	5/14	12/11
Ethnicity(Caucasian /Non-Caucasian)	15/4	22/1

2.2 Methods

2.2.1 Data acquisition

A 3T Philips Achieva Magnetic Resonance System was used. DTI data were acquired using a single-shot echo-planar imaging (EPI) sequence with SENSE parallel imaging scheme (SENSitivity Encoding, reduction factor = 2.3). The imaging matrix was 112×112 with a field of view (FOV) of 224×224mm (nominal resolution of 2mm), which was zero filled to 256×256. Axial slices of 2.2 mm thickness were acquired parallel to the anterior-posterior commissure (AC-PC) line. A total of 60 slices covered the entire hemisphere and brainstem without a gap. The echo time (TE) and repetition time (TR) were 97ms and 7.6 s, respectively, without cardiac gating. The diffusion weighting was encoded along 30 independent orientations and the b value was 1000s/mm^2 (Jones, Horsfield, & Simmons, 1999).Imaging time for each sequence was 5 minutes and 15 seconds. To increase the signal-to-noise ratio (SNR), two repetitions were performed, with a total imaging time of 12 minutes. Co-registered three-dimensional

magnetization-prepared rapid acquisition gradient echo (3D-MPRAGE) images were also obtained with the same field of view (FOV) as that in diffusion tensor imaging.

2.2.2 Data processing and analysis

Quantitative comparison at multiple levels: Why voxel-wise, cluster analysis and tract-level/along tract analysis were used?

The voxel-wise comparison between groups is performed using randomise option of TBSS. No voxels where identified that have significant difference in FA between groups that withstood the whole-brain correction for multiple comparisons. Several voxels that have a FA difference between the groups were identified that are not corrected for multiple comparisons. These voxels provide us the MNI coordinates and the tract information of where there is a difference between the groups. Since these voxels are not corrected for multiple comparisons there is chance that these results are false positives. The details of the TBSS steps and statistical analysis are explained in section 2.2.2.2. To avoid false positives in the results cluster analysis is conducted. In cluster analysis the uncorrected voxels identified in voxel-wise comparison are filtered to identify clusters that have at least 10 contiguous voxels and the FA value is greater than 0.2. From cluster analysis we identified clusters that have significant difference between the two groups. The details of cluster analysis are explained in section 2.2.2.3. Cluster analysis and voxel-wise analysis does not provide any information at the tract level. To identify if the entire tract is compromised or only if certain region of the tract is compromised between the two groups tract-level and along the tract analysis is conducted. In tract-level analysis the tracts are identified from deterministic atlas and probabilistic atlas. Then average FA is calculated in a particular tract for each subject and a student t test is done to see if there is a significant difference in the average between two groups. If a tract is identified where there is a significant difference an along tract analysis is performed in that particular tract to identify in which regions of the tract there is a difference in the FA. The details of how the

tract-level and along-tract analysis are conducted are explained in section 2.2.2.4. The overall data processing and analysis steps are outlined in figure 2.1.

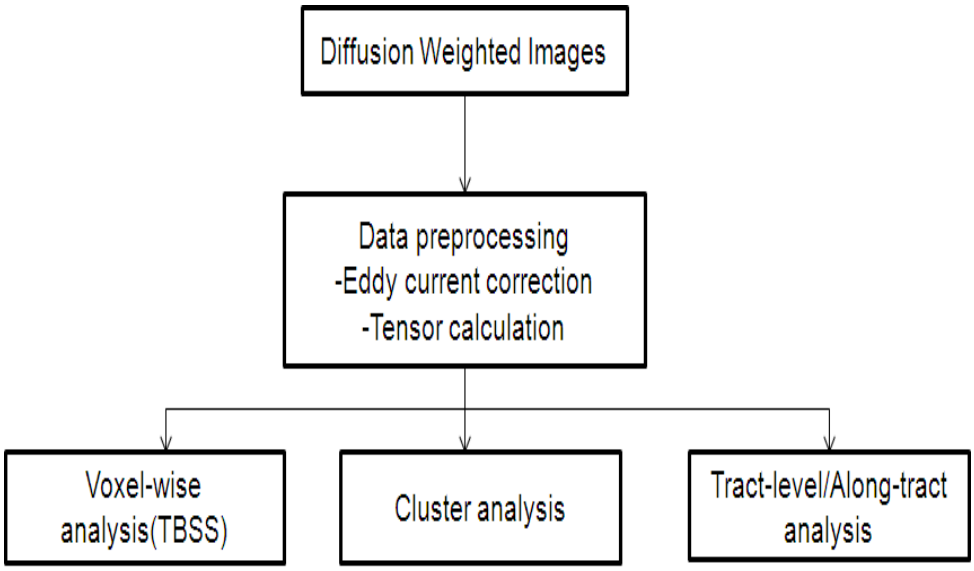

Figure 2.1 Data processing and analysis steps

2.2.2.1 Data preprocessing

All the acquired diffusion weighted images are processed using DTI Studio open software (https://www.mristudio.org/) (Jiang, van Zijl, Kim, Pearlson, & Mori, 2006). To correct the distortions caused by eddy current and motion, automated image registration (AIR) (Woods, Grafton, Holmes, Cherry, & Mazziotta, 1998) was performed on the raw images. DTI matrix for each voxel element was calculated based on multivariate linear least square fit. The tensor matrix was then diagonalized to derive principal eigenvalues (λ_{1-3}) and eigenvectors (ν_{1-3}). Maps of diffusion metrics, namely, fractional anisotropy (FA), mean diffusivity (MD mm^2s^{-1}), axial diffusivity (AxD, $\lambda_{||}$ mm^2s^{-1}), and radial diffusivity (RD, $\lambda_{\perp}$ mm^2s^{-1}), were obtained. The images are then down sampled and a resolution of 1.75x1.75sx1.75 mm^3 is achieved using IDL software.

2.2.2.2 Voxel-wise comparison

To localize brain changes related to disease between groups, voxel-wise statistical analysis is performed on the diffusion weighted images. Voxel wise analysis of diffusion weighted images was performed using software package tract based spatial statistics (TBSS, FMRIB Software Library, FMRIB Center, Oxford, United Kingdom) (Smith et al., 2006). The first step in the TBSS processing is to align all the fractional anisotropy maps of the subjects to a common target. To better incorporate the information in the digital white matter atlas developed at Johns Hopkins University, the JHU ICBM-DTI-81 (Mori et al., 2008) is used as the target image instead of the common FA target image (Huang, Fan, Weiner, et al., 2011). All the subjects' FA data is transformed into JHU ICBM-DTI-81 space. After nonlinear registration, the entire aligned dataset was transferred by affine transformation and zero padded into the ICBM-DTI-81 space which has the labeling of white matter structures and dimension of 182 x 218x182 with 1x1x1 mm^3 resolution. The registered FA images are averaged to create a mean FA (mean_FA) image. From the mean_FA image a skeleton is generated which represents the tracts that are common to all subjects. In the skeleton the tracts are represented as lines or surface as shown in the figure 2.2.

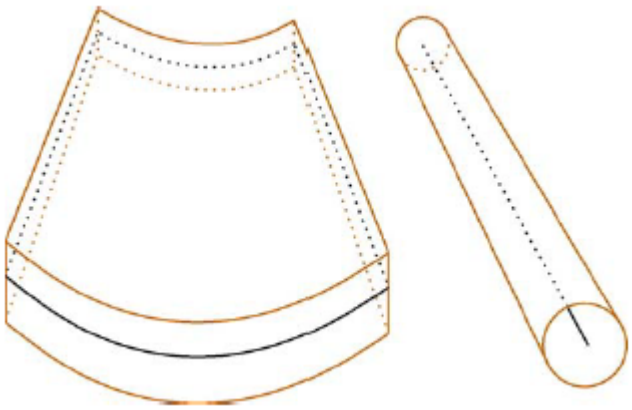

Figure 2.2: Tract representation in the skeleton.

The FA will be maximum along the surface or the lines of the skeleton and decreases as we move away from the skeleton. To get the skeleton the first step is to estimate the local

surface perpendicular direction and then perform non-maximum-suppression in this direction. The local tract surface orientation is obtained by finding the center of gravity of the local 3x3x3 voxel neighborhood. The vector from the current voxel to the local center of gravity will point towards the tract center, in a direction perpendicular to the local tract structure. As long as the local center of gravity is greater than 0.1mm the vector gives the perpendicular direction as shown in figure 2.3.

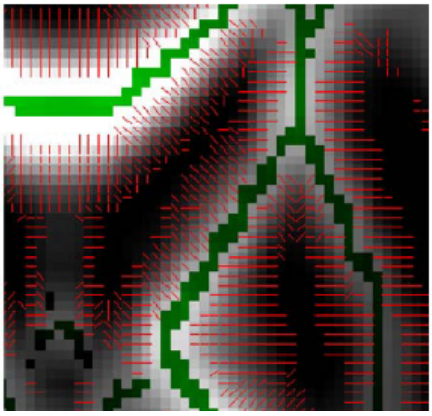

Figure 2.3 Skeletonisation using local FA center-of-gravity to find tract perpendiculars.

When the local center of gravity is less than 0.1mm, in a 3x3x3 voxel neighborhood, the mean of each opposing pair of voxels is subtracted from the center value and the direction which has maximum difference in the FA is assumed to be the perpendicular to the local tract as shown in the figure 2.4.

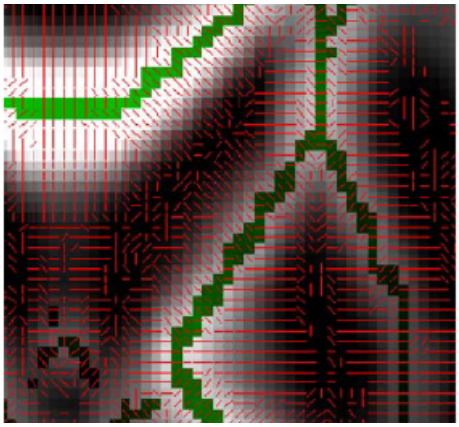

Figure 2.4 Skeletonisation using maximum FA difference to find tract perpendiculars.

Once the local tract surface orientation is identified, at each voxel then we compare the FA value with the two closest neighbor voxels on each side in the direction of the tract perpendicular. If FA value is greater than the neighbor values, that voxel is marked to be on the skeleton. The skeleton is then thresholded for FA greater than 0.2 to exclude any voxels that are primarily grey matter or CSF and does not belong to the outermost edges of the cortex. Each subject's aligned FA images are projected on to the mean FA skeleton to create a four dimensional skeletonised image that represents each subject's FA data along the skeleton. This step accounts for the residual misalignments between subjects after the initial nonlinear registration. Two constraints are placed on the aligned FA images when performing the perpendicular search to assign FA values to the skeleton. The first constraint is the search remains closer to the starting section of skeleton when two skeleton tracts are close to each other. The amount of search area is determined by the distance map, the voxels in the distance map are filled with values encoding the distance to the nearest skeleton point. The search is performed only outwards from a given skeleton point while the distance measure is increasing and this ensures that any given voxel can be mapped only into a single section of the skeleton. The second constraint is a Gaussian function with full width half maximum of 20mm is applied as a multiplicative weighting to FA values when searching for maximum FA in the aligned images. Once optimal FA value is found it is assigned to the current skeleton voxel. Thus a four dimensional skeletonised image is generated with the user id as the fourth dimension and this skeletonised image is used for further statistical analysis.

To identify the FA differences between the groups of data under study, voxel-wise statistical analysis is performed on the skeletonised FA data by using randomize of TBSS. We included a cluster-based thresholding with a threshold of $T \geq 3.0$; $P<0.001$ uncorrected; number of permutations, 5000. To account for the Type-I errors: family-wise error correction with in randomize is used, which accepts the voxels that have $p<0.05$. Voxel-wise analysis is also

computed for the other DTI metrics, axial diffusivity (AxD), radial diffusivity (RD) and mean diffusivity (MD). Outline of TBSS voxel-wise analysis steps are shown in figure 2.5.

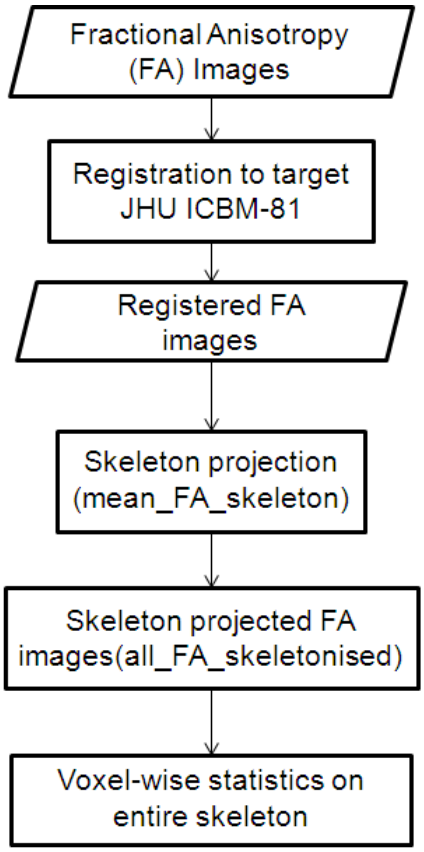

Figure 2.5 Flow chart of TBSS voxel-wise analysis

2.2.2.3 Cluster analysis

In this study, skeletonisation registration and statistical analysis of TBSS were incorporated as part of our atlas based biomarker analysis. Hence, both tract level and voxel level of comparisons were conducted. Tract level comparison has been explained in section 2.2.2.4. For voxel level comparison, the results of statistical analysis of TBSS were served as guidance or regions-of-interests of the possible disrupted white matter regions. The clusters from statistical analysis results of TBSS were further screened with the following two criteria. 1) The size of continuous voxels of the cluster has to be greater than 10. This is to prevent false

positive outcomes with the small clusters. 2) To account for the Type-I errors, a stringent P< 0.001 (uncorrected) was used (Cullen et al; Versace et al). This criterion has been tested to be able to stand for a small volume correction. And this small volume is usually 100 times the number of voxels than each cluster (Cullen et al; Versace et al). However, a more stringent whole brain correction was not adopted as such correction failed to show significance of any cluster. Once the clusters are identified average FA was computed for individual subject on the skeletonised data in the region of interest. Student t-test is conducted comparing the patient group average to the controls.

2.2.2.4 Tract-level and along the tract analysis

Tract-level analysis was also performed in addition to the voxel-wise analysis to see if the entire white matter tract is disrupted. For the tract-level analysis two types of digital white matter atlas in the JHU ICBM-DTI 81 space are used. The first type of atlas only covers the core white matter tracts which are identified with unique numbers. The second type of atlas is featured with continuous probabilistic labeling from 0 to 100% and each tract is represented by an image volume. To ensure that the core and peripheral white matter tracts are covered a threshold of 10% was applied to the second type of atlas to binarize the probabilistic labeling and the resultant binary image volume was used as the mask for tract level analysis. Using the entire core white matter tract and the probabilistic tract as masks, the average FA values of subjects' along a tract are calculated from the skeletonised FA data (all_FA_skeletonised) provided by TBSS. In order to see if the entire tract is disrupted, student t tests were performed with these averaged values of FA. The entire white matter tract was considered to be possibly disrupted if it contained filtered significant clusters revealed by cluster analysis. If a significant difference in the FA is found along any particular tract then a detailed tract level analysis is performed by segmenting the tract slice wise. The segmentation of the tract is done depending up on the orientation of the tract. The coronal slices along the tract are considered if the tract is connecting the anterior and posterior regions. Axial slices are considered if the tract is

connecting the superior and inferior regions of the brain. The probabilistic white matter atlas is used to determine the region of interest in that particular slice to calculate the mean and standard deviation of FA. A graph is plotted with slice location from MNI coordinates on the x-axis and the calculated average FA and standard deviation on the y-axis. From the plot we can clearly identify the regions where there is a major difference in the FA values between the two groups.

CHAPTER 3

RESULTS

The results of the voxel-wise analysis, cluster analysis, tract-level analysis and along tract analysis for the two clinical groups studied are presented below.

3.1 Childhood Maltreatment results

3.1.1 Voxel-wise analysis results

Tract-based spatial statistics identified several portions of white matter that have lower FA in maltreated compared to the control. The regions with reduced FA include right cingulum projecting to hippocampus (CG-R), left inferior fronto-occipital fasciculus (IFO-L), and forceps major of corpus callosum (Fmajor), left and right superior longitudinal fasciculus (SLF-L/R). There are four clusters in the SLF-L tract (SLF-L1, SLF-L2, SLF-L3 and SLF-L4). The axial, coronal and sagittal locations of white matter tract regions that showed significant difference between the two groups are shown in figure 3.1. In figure 3.1 the underlying gray scale images are the MNI152 FA maps, the green color indicated the core white matter skeleton and red color clusters indicate where there is a significant difference ($p<0.001$) in FA between the control and maltreated children. White cross hairs indicate the clusters of the specified white matter tracts if multiple clusters are shown in the image.

Voxel-wise analysis results of AxD that are identified by the randomise statistics of TBSS. Clusters with decreased AxD in maltreated are observed on the right and left superior longitudinal fasciculus (SLF-R/L) and Inferior fronto-occipital fasciculus right (IFO-R). Figure 3.2, shows the white matter tract region where there is a difference in axial diffusivity. In figure 3.2 the underlying gray scale images are the MNI152 FA maps, the green color indicated the core white matter skeleton and red color clusters indicate where there is a significant difference

(p<0.001) in FA between the control and maltreated children. White cross hairs indicate the clusters of the specified white matter tracts if multiple clusters are shown in the image.

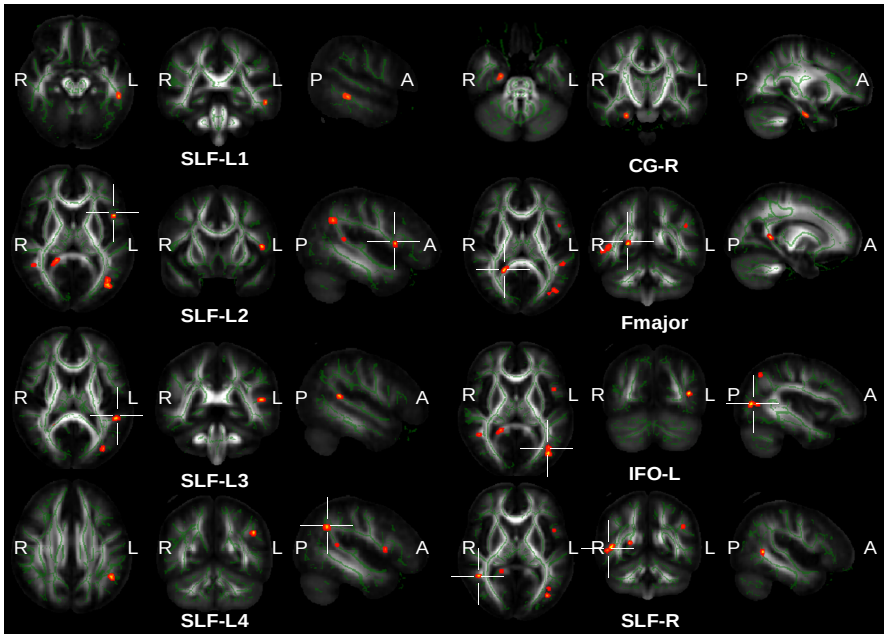

Figure 3.1: Childhood Maltreatment voxel-wise analysis results of FA.

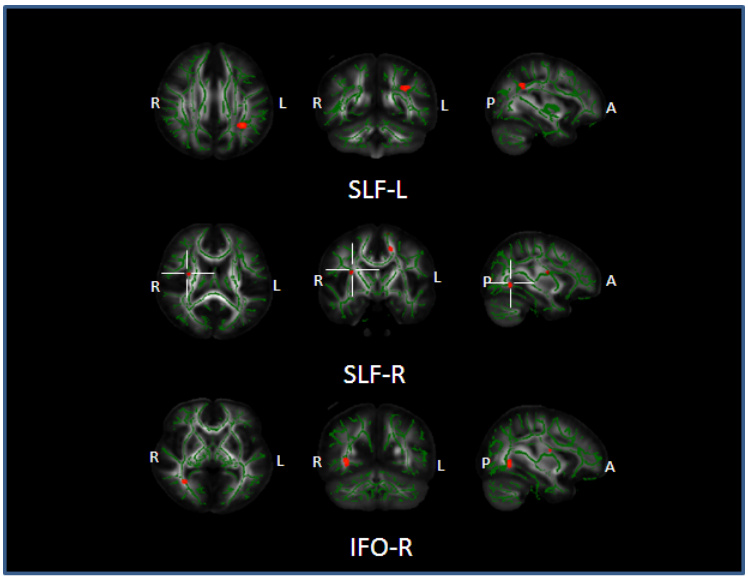

Figure 3.2 Childhood Maltreatment voxel-wise analysis results of AxD.

Tract-based spatial statistics identified several portions of white matter that have higher radial diffusivity in maltreated compared to the control. The regions with increased RD include right uncinate fasciculus /right inferior longitudinal fasciculus (UF/ILF-R), forceps major of corpus callosum (Fmajor), left and right inferior fronto-occipital fasciculus (IFO-L/R), right anterior thalamic radiation (ATR-R), and left superior longitudinal fasciculus (SLF-L). The axial, coronal and sagittal locations of white matter tract regions that showed significant difference between the two groups are shown in figure 3.3. In figure 3.3 the underlying gray scale images are the MNI152 FA maps, the green color indicated the core white matter skeleton and red color clusters indicate where there is a significant difference ($p<0.001$) in FA between the control and maltreated children. White cross hairs indicate the clusters of the specified white matter tracts if multiple clusters are shown in the image.

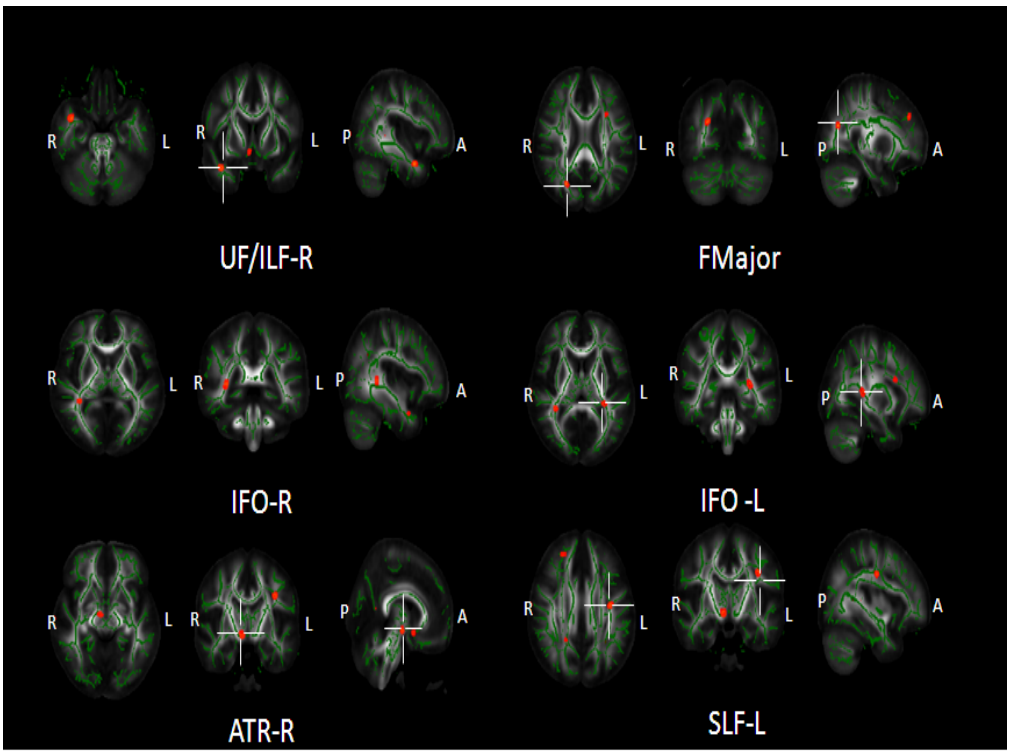

Figure 3.3 Childhood Maltreatment voxel-wise analysis results of RD

A cluster with greater mean diffusivity in maltreated compared to control was observed on left superior longitudinal fasciculus (SLF-L) by the tract based spatial statistics. The axial, coronal and sagittal slices showing the location of the cluster are shown in figure 3.4. In figure 3.4 the underlying gray scale images are the MNI152 FA maps, the green color indicated the core white matter skeleton and red color clusters indicate where there is a significant difference ($p<0.001$) in FA between the control and maltreated children. White cross hairs indicate the clusters of the specified white matter tracts if multiple clusters are shown in the image.

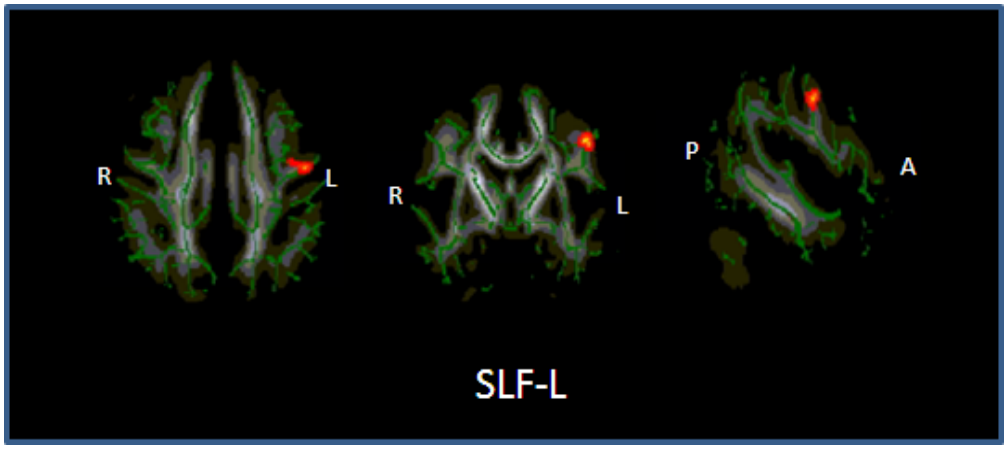

Figure 3.4 Childhood Maltreatment voxel-wise analysis results of MD

3.1.2 Cluster analysis

Using the statistics results from TBSS as guidance large clusters with contiguous voxels of greater than 10 were identified using software developed in IDL. Cluster analysis was performed on all the clusters isolated for all the DTI metrics FA, AxD, RD and MD to avoid false positives as explained in the methods. The mean, standard deviation, number of voxels in each cluster and the p values are all tabulated for each of the DTI metrics. Table 3.1 has the cluster analysis results of the FA. The results of AxD, RD and MD are tabulated in tables 3.2, 3.3 and 3.4 respectively. All the data is represented as mean and standard deviations or as raw values.

Table 3.1 Childhood Maltreatment cluster analysis results of FA

Tract Name	Control (n=13)	Maltreated (n=19)	#Voxels	p
Superior Longitudinal Fasciculus (R)	0.49 ± 0.05	0.39 ± 0.09	16	.0001
Superior Longitudinal Fasciculus (L)	0.43 + 0.03	0.34 + 0.04	67	.0001
Cluster 1	0.32 ± 0.04	0.25 ± 0.04	21	.0001
Cluster 2	0.40 ± 0.05	0.32 ± 0.07	15	.0002
Cluster 3	0.45 ± 0.05	0.38 ± 0.05	15	.0001
Cluster 4	0.50 ± 0.07	0.39 ± 0.08	16	.0002
Cingulum-Hippocampus Projection (R)	0.32 ± 0.05	0.25 ± 0.04	35	.0001
Inferior Fronto-occipital Fasciculus (L)	0.51 ± 0.06	0.39 ± 0.07	41	.0001
Forceps Major	0.72 ± 0.06	0.59 ± 0.09	21	.0001

Table 3.2 Childhood Maltreatment cluster analysis results of AxD

Tract Name	Control (n=13) mm^2/s	Maltreated (n=19) mm^2/s	#Voxels	p
Superior Longitudinal Fasciculus (R)	0.0012±0.0003	0.0009 ± 0.00007	14	<0.0001
Superior Longitudinal Fasciculus (L)	0.0011 ± 0.0001	0.00089 ± 0.00005	26	0.0003

Table 3.2 - *Continued*

Inferior Fronto-occipital Fasciculus (R)	0.0009 ± 0.00005	0.00081 ± 0.00004	20	<0.0001

Table 3.3 Childhood Maltreatment cluster analysis results of RD

Tract Name	Control (n=13) mm^2/s	Maltreated (n=19) mm^2/s	#Voxels	p
Uncinate Fasciculus/Inferior Longitudinal Fasciculus (R)	0.00053±0.00007	0.00064±0.00006	16	<.0001
Forceps Major	0.00054±0.00008	0.00066±0.0001	12	.0008
Inferior Fronto-occipital Fasciculus (R)	0.00049±0.00004	0.00058±0.0006	11	<.0001
Inferior Fronto-occipital Fasciculus (L)	0.00036±0.00002	0.00054±0.0001	11	.0006
Anterior Thalamic Radiation (R)	0.00078±0.0002	0.0011±0.0002	12	.0002
Superior Longitudinal Fasciculus (L)	0.0005±0.0004	0.00058±0.0001	12	.0005

Table 3.4 Childhood Maltreatment cluster analysis results of MD

Tract Name	Control (n=13) mm^2/s	Maltreated (n=19) mm^2/s	#Voxels	p

Table 3.4 - *Continued*

Superior Longitudinal Fasciculus (L)	0.002+0.00007	0.0021+0.00007	32	0.0005

3.1.3 Tract-level analysis results

In the tract-level analysis only superior longitudinal fasciculus left (SLF-L) showed a significant difference in FA between the childhood maltreatment group and the control subjects (p= 0.038). There is a decrease in FA for the subjects exposed to maltreatment in the childhood suggesting that several regions of the tract are disrupted.

None of the DTI metrics AD, RD and MD showed any significant tract level disruption when the entire white matter tract is considered. This indicates that only certain regions of the tract are more disrupted.

3.1.4 Along the tract analysis results

The left superior longitudinal fasciculus (SLF-L) was segmented into two parts, the superior and inferior one, by an axial plane at z=90 in MNI coordinate as shown in figure 3.5. For the superior and inferior part, the cross-section of a sequential coronal and axial planes and the white matter mask from probabilistic atlas was used as ROI to calculate the mean and standard deviation of FA in the sequential planes, respectively.

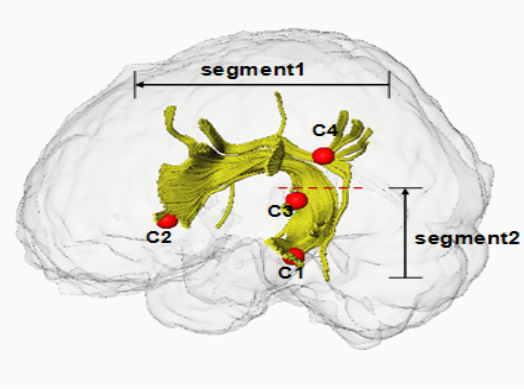

Figure 3.5: The reconstructed SLF-L and the four clusters with significant FA are represented by red dots. SLF-L segmented into superior and inferior regions at axial plane z =90 in MNI coordinates.

The FA average and standard deviation of the maltreated children and healthy control subjects along the coronal and axial slices are shown in figure 3.6.

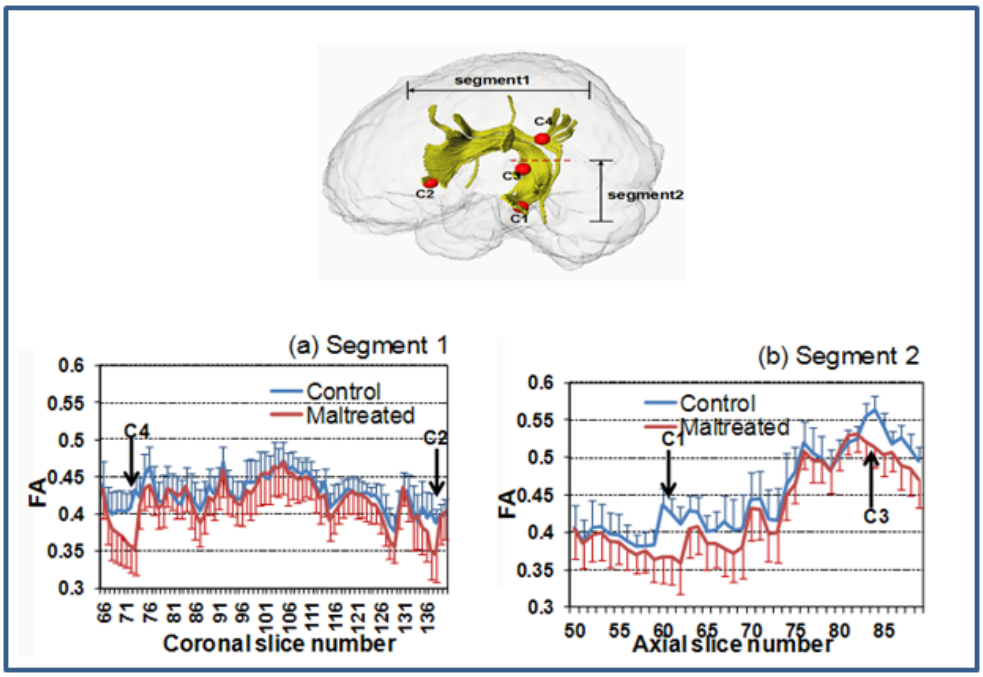

Figure 3.6: FA profiles of the segment 1 (a) and segment 2 (b) of left superior longitudinal fasciculus. Dramatic FA differences between maltreated and control group in the FA profile coincide with the locations of disrupted clusters (C1, C2, C3 and C4).

3.2 Amnestic Mild Cognitive Impairment results

3.2.1 Voxel-wise analysis results

Tract-based spatial statistics identified several portions of white matter that have lower FA in aMCI compared to the control. The regions with reduced FA include left cingulum projecting to hippocampus (CGH-L), left fornix (FX-L), left uncinate and inferior fronto-occipital fasciculus (UNC-IFO-L), right superior longitudinal fasciculus (SLF-R) and left superior corona radiate (SCR-L) The axial, coronal and sagittal locations of white matter tract regions that showed significant difference between the two groups are shown in figure 3.7. In figure 3.7

the underlying gray scale images are the MNI152 FA maps, the green color indicated the core white matter skeleton and red color clusters indicate where there is a significant difference ($p<0.001$) in FA between the control and maltreated children. White cross hairs indicate the clusters of the specified white matter tracts if multiple clusters are shown in the image.

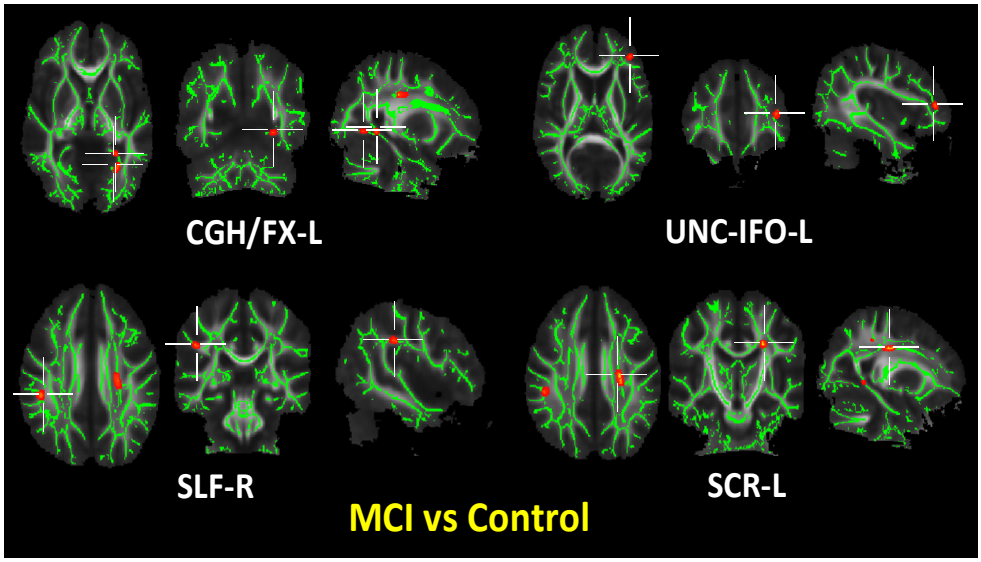

Figure 3.7 aMCI voxel-wise analysis results of FA

The tract-based spatial statistics identified a cluster on left superior corona radiate that has significant difference in the axial diffusivity between aMCI compared to the control subjects as shown in figure 3.8. In figure 3.8 the underlying gray scale images are the MNI152 FA maps, the green color indicated the core white matter skeleton and red color clusters indicate where there is a significant difference ($p<0.001$) in FA between the control and maltreated children. White cross hairs indicate the clusters of the specified white matter tracts if multiple clusters are shown in the image.

Three major clusters on Right cingulum projecting on to hippocampus (CGH-R), right inferior fronto-occipital fasciculus (IFO-R), left superior corona radiate (SCR-L) with reduced radial diffusivity in controls compared to the aMCI were identified by the tract-based spatial statistics. The axial, coronal and sagittal slices with the location of clusters are shown in figure 3.9. In figure 3.9 the underlying gray scale images are the MNI152 FA maps, the green color

indicated the core white matter skeleton and red color clusters indicate where there is a significant difference ($p<0.001$) in FA between the control and maltreated children. White cross hairs indicate the clusters of the specified white matter tracts if multiple clusters are shown in the image.

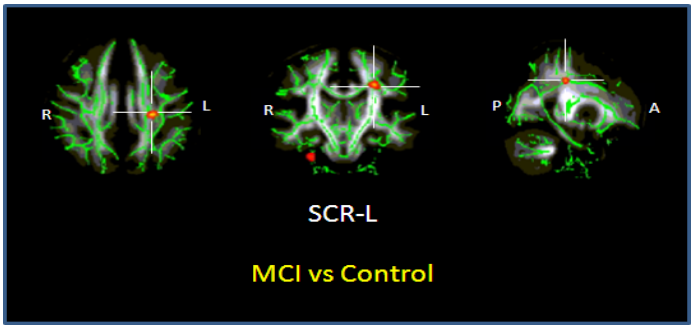

Figure 3.8 aMCI voxel-wise analysis results of AxD

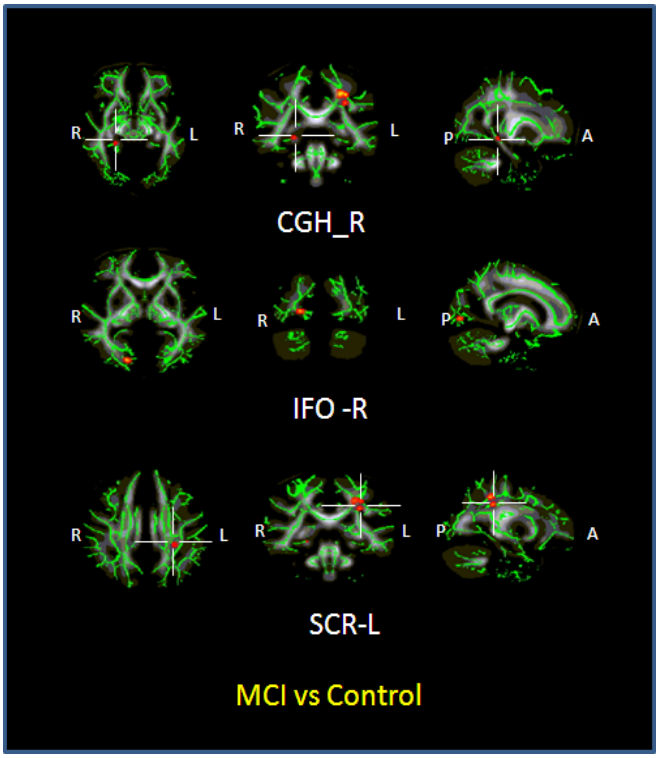

Figure 3.9 aMCI voxel-wise analysis results of RD

Tract-based spatial statistics identified several portions of white matter that have lower MD in control compared to the aMCI. The regions with increased mean diffusivity include right

cingulum projecting to hippocampus (CGH-R), left and right inferior fronto-occipital fasciculus (IFO-L/R), left cortico spinal tract (CST-L) and, left superior longitudinal fasciculus (SLF-L). There are two clusters in the SLF-L tract (SLF-L1, SLF-L2). The axial, coronal and sagittal locations of white matter tract regions that showed significant difference between the two groups are shown in figure 3.10. In figure 3.10 the underlying gray scale images are the MNI152 FA maps, the green color indicated the core white matter skeleton and red color clusters indicate where there is a significant difference ($p<0.001$) in FA between the control and maltreated children. White cross hairs indicate the clusters of the specified white matter tracts if multiple clusters are shown in the image.

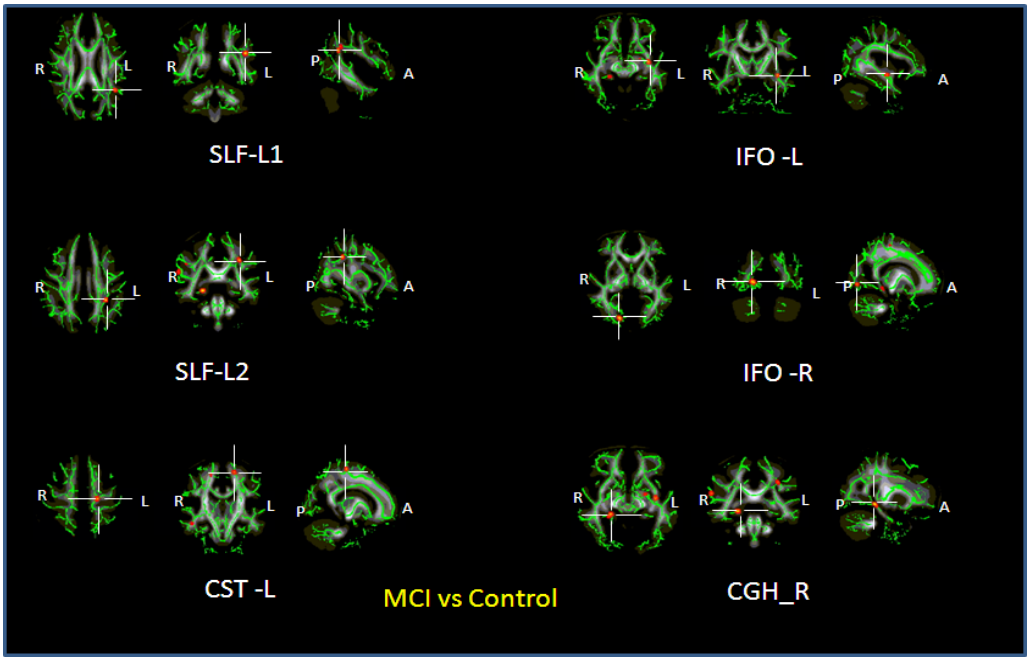

Figure 3.10 aMCI voxel-wise analysis results of MD

3.2.2 Cluster analysis results

Using the statistics results from TBSS as guidance large clusters with contiguous voxels of greater than 10 were identified using software developed in IDL. Cluster analysis was performed on all the clusters isolated for all the DTI metrics FA, AxD, RD and MD to avoid false positives as explained in the methods. The mean, standard deviation, number of voxels in each

cluster and the p values are all tabulated for each of the DTI metrics. Table 3.5 has the cluster analysis results of the FA. The results of AxD, RD and MD are tabulated in tables 3.6, 3.7 and 3.8 respectively. All the data is represented as mean and standard deviations or as raw values.

Table 3.5 aMCI Maltreatment cluster analysis results of FA

Tract Name	Control (n=19)	aMCI (n=23)	#Voxels	p
Cingulum-Hippocampus Projection (L)	0.336 ± 0.038	0.276± 0.036	21	<0.0001
Fornix (L)	0.425±0.059	0.338±0.058	16	<0.0001
Superior Corona Radiata (L)	0.435±0.048	0.382±0.044	35	0.0002
Uncinate and Inferior fronto-occipital fasciculus (L)	0.336±0.042	0.260±0.076	16	0.0002
Superior longitudinal fasciculus (R)	0.432±0.039	0.307±0.038	17	<0.0001

Table 3.6 aMCI Maltreatment cluster analysis results of AxD

Tract Name	Control (n=19) mm^2/s	aMCI (n=23) mm^2/s	#Voxels	p
Superior Corona Radiata (L)	0.00105 ±0.00004	0.00099±0.00005	18	<0.0001

Table 3.7 aMCI Maltreatment cluster analysis results of RD

Tract Name	Control (n=19) mm^2/s	aMCI (n=23) mm^2/s	#Voxels	p
Cingulum-Hippocampus Projection (R)	0.00046±0.00007	0.00053±0.00005	12	0.0008
Inferior fronto-occipital fasciculus (L)	0.00056±0.00003	0.00063±0.00006	25	<0.0001
Superior Longitudinal fasciculus (L)	0.00057±0.00003	0.00062±0.00003	16	0.0002

Table 3.8 aMCI Maltreatment cluster analysis results of MD

Tract Name	Control (n=19) mm^2/s	aMCI (n=23) mm^2/s	#Voxels	p
Superior Longitudinal Fasciculus (L)				
Cluster 1	0.0021±0.0001	0.0023±0.00008	13	<0.0001
Cluster 2	0.0021±0.00009	0.0022±0.00008	13	0.0002
Cortico Spinal Tract (L)	0.0019±0.00001	0.0021±0.0001	10	0.0001
Inferior fronto occipital fasciculus(L)	0.0022±0.0001	0.0024±0.0002	11	0.0002
Inferior fronto occipital fasciculus(R)	0.0022±0.0001	0.0024±0.0002	17	<0.0001
Cingulum-Hippocampus Projection (R)	0.0022±0.0001	0.0024±0.0002	25	<0.0001

3.2.3 Tract-level analysis results

In the tract-level analysis, none of the white matter tracts has significant difference between the aMCI and control subjects for all the DTI metrics. This indicated that only certain portion of the tracts is disrupted.

CHAPTER 4

DISCUSSION

4.1 Childhood Maltreatment

The results obtained from the voxel-wise and cluster analysis of the 19 children exposed to maltreatment who have no history of psychopathology and 13 age matched controls revealed that maltreated children have reduced FA values in SLF-L, SLF-R, CGH-R, IFO-L and F-major. The SLF-L has four regions along the tract that have reduced FA in maltreated group. In the tract-level analysis that compares the average FA of all the voxels in the tracts between two groups, SLF-L showed significant difference. The observed white matter disruptions, specifically SLF-L, SLF-R and CGH-R, were associated with increased vulnerability to unipolar depression and/or substance abuse.

The FA profile showed clusters with decreased fractional anisotropy on the superior longitudinal fasciculus (SLF) (figure 3.1, table 3.1). SLF is an association fiber known to connect frontal, parietal, and temporal cortex. Fibers originate in prefrontal and premotor gyri (mainly Broca's area) and project posteriorly to Wernicke's area. (Catani, Howard, Pajevic, & Jones, 2002). The Broca's area and Wernicke's area are known in the involvement of producing and understanding speech and language. The SLF fibers are also known to be involved in specific behavioral and cognitive functions(Schmahmann et al., 2007).It is also known that structural development of SLF continues into adulthood (Giorgio et al., 2008). Decrease in FA of right and left SLF might cause some language deficits in patients exposed to childhood maltreatment. A decrease in AD, increase in RD and MD is also observed in the SLF-L (figure 3.1, 3.2, 3.3 and 3.4; tables 3.1,3.2,3.3 and 3.4). Decrease in AD and increase in RD along with decrease in FA has been observed in secondary Wallerian degeneration (Pierpaoli et al., 2001). On the left SLF tract, four major clusters with reduced FA have been found (figure 3.1, table 3.1). The tract-wise

analysis also revealed a significant difference ($p<0.05$) in the fractional anisotropy of the left superior longitudinal fasciculus. The along tract analysis of left SLF have shown significant decrease in the FA in the maltreated subjects which are in the same location where the clusters have been identified (figure 3.6). Asymmetry and dominance of this tract in left hemisphere have been found in several studies (Catani et al., 2007). In a similar study on finding white matter tract abnormalities in young adults exposed to parental verbal abuse (Choi et al., 2009), disruption in left arcuate fasciculus, the fronto-temporal branch of SLF-L, has also been found. There have also been reports that there is decrease in FA in SLF-L for patients suffering from Major depression (Frodl et al., 2012). The exact functions of the SLF is not clear because of its wide spread connections throughout the brain and its association with maltreatment is not yet clear. In the follow-up study conducted on the subjects a correlation between the reduced FA in SLF-L and who developed pyscopathology (having a mood and/or substance use disorder) has been observed. This finding suggests that SLF-L is associated with mood or substance use disorder.

Inferior fronto-occipital fasciculus (IFO) is another association fiber that connects the inferior and lateral margins of occipital lobe to the inferolateral and dorsolateral regions of the frontal lobe. It is known to be involved in emotional and visual function (Catani et al., 2002). No cluster with significant difference in FA has been identified on the right IFO. But, there is a decrease in the axial diffusivity (figure 3.2) and increase in the radial diffusivity (figure 3.3) indicating axonal damage and demyelination of right IFO. The FA and RD profiles identified clusters on left IFO that has significant difference between the subjects exposed to childhood maltreatment and healthy controls (figure 3.1 and figure 3.3). Several studies associated with depression reported a decrease in the FA of IFO tract (Cullen et al., 2010; Huang, Fan, Williamson, & Rao, 2011). The exact association of the IFO with maltreatment has to be further studied.

In this study we also found disruption in other association fibers that include right anterior thalamic radiation (ATR) and right uncinate/ inferior longitudinal fasciculus (UF/ILF). The uncinate fasciculus connects the anterior part of the temporal lobe with orbital lobe and polar frontal cortex. The ILF is known to connect the temporal lobe with the occipital lobe (Catani et al., 2002). The exact function of uncinate is unknown but it is possible that it might be involved in emotion processing, memory and language functions (Catani & Thiebaut de Schotten, 2008). The inferior longitudinal fasciculus is involved in face recognition, visual perception, reading, visual memory and other functions related to language (Catani & Thiebaut de Schotten, 2008). Anterior thalamic radiation has fibers that connect the thalamus with the frontal cortex. The structural abnormalities in ATR are linked to the dysfunction in executive processes and declarative memory (Van der Werf, Jolles, Witter, & Uylings, 2003). The radial diffusivity profile showed clusters on right ATR and right UF/ILF (figure 3.3, table 3.3) with an increase in the RD. This indicates that there is demyelination in the tracts. However, there association with the maltreatment is not well understood and needs more investigation.

The corpus callosum is the largest commissural projection in the central nervous system and it is conventionally divided in to genu, body and splenium. Splenium is known to connect the occipital lobes of the two hemispheres and it also arc out forming forceps major (Catani & Thiebaut de Schotten, 2008). The splenium is known to communicate somatosensory information between the two halves of the occipital lobe. The results show a decrease in the FA and increase in the RD in Fmajor (figures 3.1, 3.3). This suggests there is a demyelination in the tract. Several DTI studies on depression found a decrease in the FA of the corpus callosum (Kieseppa et al., 2010; Maller et al., 2010; Sexton, Mackay, & Ebmeier, 2009). There is no direct connection between the disruption of forceps major and childhood maltreatment. But the results suggest that kids exposed to maltreatment might be at higher risk for developing depression.

The FA profile also shows a cluster with decreased FA on right cingulum (figure 3.1). The cingulum bundle is one of the prominent limbic fiber tracts. It connects the regions of cortex (medial frontal, parietal, occipital, and temporal lobes) to cingulate gyrus. It is known to be involved in attention, memory and emotions. (Rudrauf, Mehta, & Grabowski, 2008, Catani, 2006 #305).

In conclusion, white matter tract disruptions were observed in adolescents exposed to maltreatment during childhood, and these disruptions were associated with increased vulnerability to unipolar depression and substance use disorder. The significant changes in the SLF-L tract and its correlation with the development of mood or substance abuse disorders also suggest that this tract could be used as clinical biomarker in early identification of children who might be at risk of developing mood disorders. The findings have potential implications for identifying youngsters at highest risk for these disorders and targeted preventive interventions.

4.2 Amnestic Mild Cognitive Impairment

The results obtained after analyzing the data from 23 aMCI patients and 19 age matched controls revealed several clusters that showed difference in the DTI metrics in the limbic, association and projection fiber tracts between the two groups. All the differences are localized to particular region of the tract and hence no tract-level differences were identified between the patient and control groups.

Measures from DTI metrics allow inferences about white matter microstructure in vivo by quantifying the directionality and the rate of diffusion of water within tissue. The most frequently used DTI metric is FA. The FA values range between 0 and 1, with higher values reflecting increased directionality of diffusion. The directionality of the diffusion depends on the density of physical obstruction such as membranes and the distribution of water molecules between different cellular compartments. Thus, FA is typically higher in white matter, in which diffusion is restricted by myelin sheaths of axons (Madden et al., 2012). From the results, reduction in FA alone is observed in left cingulum projecting on to hippocampus (CGH-L), left

fornix (FX-L) and left uncinate fasciculus (UNC-L) and right superior longitudinal fasciculus (SLF-R) (Figure 3.7 and Table 3.5). Conceivably, this reflects mild microstructural alterations, such as minor fiber loss without gross tissue loss leading to lowered FA. (Rovaris & Filippi, 2007; Sen & Basser, 2005)

Disruption of the limbic tracts in AD has been most widely reported (Stahl et al., 2007; Takahashi et al., 2002; Zhang et al., 2007{Xie, 2006 #100). Degeneration of the limbic system is closely associated with AD. In the limbic system network, atrophy of hippocampal and parahippocampal regions (Stoub et al., 2006) and medial temporal lobe (Thompson et al., 2003) are well documented. The fornix is a WM tract connecting the hippocampus with the septal region, mammillary bodies, and prefrontal cortex (Zhuang et al., 2010). Previous DTI studies have found reduced fornix integrity and its association with hippocampal atrophy in Alzheimer's disease (DeCarli et al., 2008; Y. W. Liu et al., 2011; Liu et al., 2009;Teipel et al., 2007). Therefore, the presence of fornix degradation in our aMCI subjects probably stems from Wallerian degeneration secondary to hippocampal atrophy, thus indirectly reflecting hippocampal damage which is a hallmark of AD pathology. More importantly, the disrupted connectivity between hippocampus and prefrontal cortex via fornix can cause memory dysfunction, such as abnormal memory organization and reduced overall episodic memory (Nestor et al., 2007; Takei et al., 2008). Therefore, the disruption of fornix found in our study further supports the well-established notion that medial temporal memory system is affected early in the preclinical AD stage (Dickerson, 2004 #288).Cingulum has fibers of different lengths connecting the temporal gyrus to the orbitofrontal cortex. Some of the fibers connect the medial frontal, parietal, occipital and temporal lobes and different portions of cingulated cortex. Cingulum is also known to be involved in attention, memory and emotional functions (Catani, 2006). The posterior cingulum is an important hub which sustains information transfer between the parahippocampal gyrus and the prefrontal cortex and damage to this area leads to dysfunction of a network that is responsible for sustaining memory function. (Vincent et al.,

2006). Reduced white matter volume in the cingulum (Villain et al., 2008) has also been reported. DTI studies on MCI patients also found that only left cingulum is affected compared to the control. (Fellgiebel et al., 2008; Medina et al., 2006; Zhang et al., 2007).

Left Uncinate fasciculus and the right SLF are the association fiber tracts. The SLF connects different regions of the cortex. It is known to be involved in the language and speech processing but its wide range of connections suggests SLF might be involved in wide range of functions. (Catani, 2006) The uncinate fasciculus connects the hippocampus to the subgenual cortex (O'Dwyer et al., 2011).Other studies on Alzheimer's that are based on DTI data also found disruption in the association fiber tracts (e.g. (Fellgiebel et al., 2008; Xie et al., 2006)). In several AD studies a reduced FA is observed in bilateral superior longitudinal fasciculus, inferior longitudinal fasciculus, uncinate fasciculus, cingulum bundles, corticospinal tracts and corpus callosum (e.g.:C. L. Liu, Bammer, & Moseley, 2003; Shu, Wang, Qi, Li, & He, 2011; Stricker et al., 2009).

A cluster with decreased FA, decreased AxD and increased RD was identified in left superior corona radiate (Figure 3.7, 3.8 and 3.9). The corona radiata contains pathways devoted primarily to motor and somatosensory function (Gebauer et al., 2011).This type of diffusivity pattern has been observed in secondary (Wallerian) degeneration, which is the degeneration, over time, of axon fibers distal to the point of transection or injury. (Sun, Liang, Cross, & Song, 2008, Pierpaoli et al., 2001 , Cohen-Adad et al., 2011). This process involves initial axonal beading, organelle accumulation, and finally the breakdown of myelin and oligodendrocyte apoptosis. The cellular debris is cleared by activated microglia and glial scar is formed by astrocytes (Vargas & Barres, 2007). This glia infiltration, which restricts AD and decreases MD differentiates Wallerian degeneration from mere loss of fibers and myelin (Wang et al., 2009). The similar kind of pattern was observed by Bennett et al and Burzynska et al. in older adults. This indicates that SCR degeneration is common with aging but from the results obtained it is more prominent in patients diagnosed with amnestic MCI.

An increase in RD and MD are observed in right cingulum projecting on to hippocampus and the right inferior fronto-occipital fasciculus. Similar DTI metric changes, in bilateral cingulum and IFO are observed in a study conducted by Bosch et al (2012) on AD patients. Usually a decrease in FA associated with an increase in RD and increase in MD is known to be associated with demyelination. But, just increase in RD indicates that there is some disruption in the white matter tract but does not provide more information about the alterations in the white matter microstructures. Changes in only MD are observed in the left SLF and left CST which are association and projection tracts respectively.

From the results obtained from the aMCI study and the widely documented AD results we can see a similar trend in the white matter changes of the patients. The changes in the limbic fiber tracts are more correlated with the changes observed in AD patients. The association of the limbic tracts with memory function and the regional disruption observed in the cingulum and fornix indicates that these tracts could be used as clinical biomarkers to identify the progression of aMCI to AD.

CHAPTER 5

CONCLUSION

Based on the results obtained we found white matter abnormalities in patient groups, maltreated children and amnestic MCI.

The results of Childhood Maltreatment indicate that any form of abuse will have its impact on the white matter structures. Abnormalities were identified in the association fibers and callosal fibers. These disruptions were associated with increased vulnerability to unipolar depression and substance use disorder. The findings have potential implications for identifying youngsters at highest risk for these disorders and targeted preventive interventions.

In the amnestic Mild Cognitive Impairment study we found decreased FA in the limbic fibers. Disruptions in these tracts are widely observed in the Alzheimer's studies. We also identified damage in the association fibers that are involved in the emotional processing. These findings suggest that we can use diffusion tensor imaging data as a potential clinical biomarker to identify the early onset of the Alzheimer's disease.

REFERENCES

Andersen, S. L., & Teicher, M. H. (2008). Stress, sensitive periods and maturational events in adolescent depression. *Trends in Neurosciences, 31*(4), 183-191. doi: DOI 10.1016/j.tins.2008.01.004

Andreasen, N. C., Endicott, J., Spitzer, R. L., & Winokur, G. (1977). The family history method using diagnostic criteria. Reliability and validity. [Comparative Study Research Support, U.S. Gov't, Non-P.H.S.]. *Arch Gen Psychiatry, 34*(10), 1229-1235.

Azevedo, F. A. C., Carvalho, L. R. B., Grinberg, L. T., Farfel, J. M., Ferretti, R. E. L., Leite, R. E. P., . . . Herculano-Houzel, S. (2009). Equal Numbers of Neuronal and Nonneuronal Cells Make the Human Brain an Isometrically Scaled-Up Primate Brain. *Journal of Comparative Neurology, 513*(5), 532-541. doi: Doi 10.1002/Cne.21974

Basser, P. J., Mattiello, J., & LeBihan, D. (1994). MR diffusion tensor spectroscopy and imaging. *Biophys J, 66*(1), 259-267. doi: 10.1016/S0006-3495(94)80775-1

Blakemore, S. J., Burnett, S., & Dahl, R. E. (2010). The role of puberty in the developing adolescent brain. [Research Support, N.I.H., Extramural Research Support, Non-U.S. Gov't Review]. *Hum Brain Mapp, 31*(6), 926-933. doi: 10.1002/hbm.21052

Bosch, B., Arenaza-Urquijo, E. M., Rami, L., Sala-Llonch, R., Junque, C., Sole-Padulles, C., . . . Bartres-Faz, D. (2012). Multiple DTI index analysis in normal aging, amnestic MCI and AD. Relationship with neuropsychological performance. [Research Support, Non-U.S. Gov't]. *Neurobiology of Aging, 33*(1), 61-74. doi: 10.1016/j.neurobiolaging.2010.02.004

Brenhouse, H. C., & Andersen, S. L. (2011). Developmental trajectories during adolescence in males and females: a cross-species understanding of underlying brain changes. [Research Support, N.I.H., Extramural Review]. *Neurosci Biobehav Rev, 35*(8), 1687-1703. doi: 10.1016/j.neubiorev.2011.04.013

Catani, M. (2006). Diffusion tensor magnetic resonance imaging tractography in cognitive disorders. [Review]. *Curr Opin Neurol, 19*(6), 599-606. doi: 10.1097/01.wco.0000247610.44106.3f

Catani, M., Allin, M. P., Husain, M., Pugliese, L., Mesulam, M. M., Murray, R. M., & Jones, D. K. (2007). Symmetries in human brain language pathways correlate with verbal recall. [Research Support, Non-U.S. Gov't]. *Proc Natl Acad Sci U S A, 104*(43), 17163-17168. doi: 10.1073/pnas.0702116104

Catani, M., Howard, R. J., Pajevic, S., & Jones, D. K. (2002). Virtual in vivo interactive dissection of white matter fasciculi in the human brain. [Clinical Trial Research Support, Non-U.S. Gov't]. *Neuroimage, 17*(1), 77-94.

Catani, M., & Thiebaut de Schotten, M. (2008). A diffusion tensor imaging tractography atlas for virtual in vivo dissections. [Research Support, Non-U.S. Gov't]. *Cortex, 44*(8), 1105-1132. doi: 10.1016/j.cortex.2008.05.004

Cohen-Adad, J., El Mendili, M. M., Lehericy, S., Pradat, P. F., Blancho, S., Rossignol, S., & Benali, H. (2011). Demyelination and degeneration in the injured human spinal cord detected with diffusion and magnetization transfer MRI. *Neuroimage, 55*(3), 1024-1033. doi: DOI 10.1016/j.neuroimage.2010.11.089

Cui, Y., Wen, W., Lipnicki, D. M., Beg, M. F., Jin, J. S., Luo, S. H., . . . Sachdev, P. S. (2012). Automated detection of amnestic mild cognitive impairment in community-dwelling elderly adults: A combined spatial atrophy and white matter alteration approach. *Neuroimage, 59*(2), 1209-1217. doi: DOI 10.1016/j.neuroimage.2011.08.013

Cullen, K. R., Klimes-Dougan, B., Muetzel, R., Mueller, B. A., Camchong, J., Houri, A., . . . Lim, K. O. (2010). Altered white matter microstructure in adolescents with major depression: a preliminary study. [Research Support, N.I.H., Extramural Research Support, Non-U.S. Gov't]. *J Am Acad Child Adolesc Psychiatry, 49*(2), 173-183 e171.

De Bellis, M. D. (2002). Developmental traumatology: a contributory mechanism for alcohol and substance use disorders. *Psychoneuroendocrinology, 27*(1-2), 155-170.

DeCarli, C., Carmichael, O., Mungas, D., Reed, B., Martinez, O., Persianinova, M., . . . Fletcher, E. (2008). Hippocampal atrophy is accompanied by degeneration of fornix white matter tracts in Alzheimer's disease. *Neurology, 70*(11), A441-A442.

Enoch, M. A. (2011). The role of early life stress as a predictor for alcohol and drug dependence. *Psychopharmacology, 214*(1), 17-31. doi: DOI 10.1007/s00213-010-1916-6

Ernst, M., & Korelitz, K. E. (2009). Cerebral maturation in adolescence: behavioral vulnerability. [Review]. *Encephale, 35 Suppl 6*, S182-189. doi: 10.1016/S0013-7006(09)73469-4

Fellgiebel, A., Schermuly, I., Gerhard, A., Keller, I., Albrecht, J., Weibrich, C., . . . Stoeter, P. (2008). Functional relevant loss of long association fibre tracts integrity in early Alzheimer's disease. *Neuropsychologia, 46*(6), 1698-1706. doi: 10.1016/j.neuropsychologia.2007.12.010

Frodl, T., Carballedo, A., Fagan, A. J., Lisiecka, D., Ferguson, Y., & Meaney, J. F. (2012). Effects of early-life adversity on white matter diffusivity changes in patients at risk for major depression. *Journal of Psychiatry & Neuroscience, 37*(1), 37-45. doi: Doi 10.1503/Jpn.110028

Gold, B. T., Johnson, N. F., Powell, D. K., & Smith, C. D. (2012). White matter integrity and vulnerability to Alzheimer's disease: Preliminary findings and future directions. *Biochim Biophys Acta, 1822*(3), 416-422. doi: 10.1016/j.bbadis.2011.07.009

Gebauer, D., Fink, A., Filippini, N., Johansen-Berg, H., Reishofer, G., Koschutnig, K., . . . Enzinger, C. (2011). Differences in integrity of white matter and changes with training in spelling impaired children: a diffusion tensor imaging study. *Brain Struct Funct*. doi: 10.1007/s00429-011-0371-4

Giorgio, A., Watkins, K. E., Douaud, G., James, A. C., James, S., De Stefano, N., . . . Johansen-Berg, H. (2008). Changes in white matter microstructure during adolescence. [Research Support, Non-U.S. Gov't]. *Neuroimage, 39*(1), 52-61. doi: 10.1016/j.neuroimage.2007.07.043

Heim, C., & Binder, E. B. (2012). Current research trends in early life stress and depression: Review of human studies on sensitive periods, gene-environment interactions, and epigenetics. *Experimental Neurology, 233*(1), 102-111. doi: DOI 10.1016/j.expneurol.2011.10.032

Huang, H., Fan, X., Weiner, M., Martin-Cook, K., Xiao, G., Davis, J., . . . Diaz-Arrastia, R. (2011). Distinctive disruption patterns of white matter tracts in Alzheimer's disease with full diffusion tensor characterization. *Neurobiology of Aging*. doi: 10.1016/j.neurobiolaging.2011.06.027

Huang, H., Fan, X., Weiner, M., Martin-Cook, K., Xiao, G., Davis, J., . . . Diaz-Arrastia, R. (2011). Distinctive disruption patterns of white matter tracts in Alzheimer's disease with full diffusion tensor characterization. *Neurobiology of Aging*. doi: 10.1016/j.neurobiolaging.2011.06.027

Huang, H., Fan, X., Williamson, D. E., & Rao, U. (2011). White matter changes in healthy adolescents at familial risk for unipolar depression: a diffusion tensor imaging study. [Research Support, N.I.H., Extramural Research Support, Non-U.S. Gov't]. *Neuropsychopharmacology, 36*(3), 684-691. doi: 10.1038/npp.2010.199

Jiang, H., van Zijl, P. C., Kim, J., Pearlson, G. D., & Mori, S. (2006). DtiStudio: resource program for diffusion tensor computation and fiber bundle tracking. [Research Support, N.I.H., Extramural]. *Comput Methods Programs Biomed, 81*(2), 106-116. doi: 10.1016/j.cmpb.2005.08.004

Jones, D. K., Horsfield, M. A., & Simmons, A. (1999). Optimal strategies for measuring diffusion in anisotropic systems by magnetic resonance imaging. [Research Support, Non-U.S. Gov't]. *Magn Reson Med, 42*(3), 515-525.

Kieseppa, T., Eerola, M., Mantyla, R., Neuvonen, T., Poutanen, V. P., Luoma, K., . . . Isometsa, E. (2010). Major depressive disorder and white matter abnormalities: a diffusion tensor imaging study with tract-based spatial statistics. [Research Support, Non-U.S. Gov't]. *J Affect Disord, 120*(1-3), 240-244. doi: 10.1016/j.jad.2009.04.023

Liu, C. L., Bammer, R., & Moseley, M. E. (2003). Generalized diffusion tensor imaging (GDTI): A method for characterizing and imaging diffusion anisotropy caused by non-Gaussian diffusion. *Israel Journal of Chemistry, 43*(1-2), 145-154.

Liu, Y. W., Spulber, G., Lehtimaki, K. K., Kononen, M., Hallikainen, I., Grohn, H., . . . Soininen, H. (2011). Diffusion tensor imaging and Tract-Based Spatial Statistics in Alzheimer's disease and mild cognitive impairment. *Neurobiology of Aging, 32*(9), 1558-1571. doi: DOI 10.1016/j.neurobiolaging.2009.10.006

Madden, D. J., Bennett, I. J., Burzynska, A., Potter, G. G., Chen, N. K., & Song, A. W. (2012). Diffusion tensor imaging of cerebral white matter integrity in cognitive aging. *Biochim Biophys Acta, 1822*(3), 386-400. doi: 10.1016/j.bbadis.2011.08.003

Maller, J. J., Thomson, R. H., Lewis, P. M., Rose, S. E., Pannek, K., & Fitzgerald, P. B. (2010). Traumatic brain injury, major depression, and diffusion tensor imaging: making connections. [Research Support, Non-U.S. Gov't Review]. *Brain Res Rev, 64*(1), 213-240. doi: 10.1016/j.brainresrev.2010.04.003

McCrory, E., De Brito, S. A., & Viding, E. (2010). Research review: the neurobiology and genetics of maltreatment and adversity. [Research Support, Non-U.S. Gov't Review]. *J Child Psychol Psychiatry, 51*(10), 1079-1095. doi: 10.1111/j.1469-7610.2010.02271.x

Medina, D., DeToledo-Morrell, L., Urresta, F., Gabrieli, J. D. E., Moseley, M., Fleischman, D., . . . Stebbins, G. T. (2006). White matter changes in mild cognitive impairment and AD: A

diffusion tensor imaging study. *Neurobiology of Aging, 27*(5), 663-672. doi: DOI 10.1016/j.neurobiolaging.2005.03.026

Mori, S., Oishi, K., Jiang, H., Jiang, L., Li, X., Akhter, K., . . . Mazziotta, J. (2008). Stereotaxic white matter atlas based on diffusion tensor imaging in an ICBM template. [Research Support, N.I.H., Extramural]. *Neuroimage, 40*(2), 570-582. doi: 10.1016/j.neuroimage.2007.12.035

Mori, S., Oishi, K., Jiang, H., Jiang, L., Li, X., Akhter, K., . . . Mazziotta, J. (2008). Stereotaxic white matter atlas based on diffusion tensor imaging in an ICBM template. [Research Support, N.I.H., Extramural]. *Neuroimage, 40*(2), 570-582. doi: 10.1016/j.neuroimage.2007.12.035

Nestor, P. G., Kubicki, M., Kuroki, N., Gurrera, R. J., Nimikiewicz, M., Shenton, M. E., & McCarley, R. W. (2007). Episodic memory and neuroimaging of hippocampus and fornix in chronic schizophrenia. *Psychiatry Research-Neuroimaging, 155*(1), 21-28. doi: DOI 10.1016/j.psychresns.2006.12.020

Paus, T., Keshavan, M., & Giedd, J. N. (2008). OPINION Why do many psychiatric disorders emerge during adolescence? *Nature Reviews Neuroscience, 9*(12), 947-957. doi: Doi 10.1038/Nrn2513

Petersen, R. C. (2004). Mild cognitive impairment as a diagnostic entity. *Journal of Internal Medicine, 256*(3), 183-194.

Petersen, R. C., Doody, R., Kurz, A., Mohs, R. C., Morris, J. C., Rabins, P. V., . . . Winblad, B. (2001). Current concepts in mild cognitive impairment. *Archives of Neurology, 58*(12), 1985-1992.

Pierpaoli, C., & Basser, P. J. (1996). Toward a quantitative assessment of diffusion anisotropy. *Magnetic Resonance in Medicine, 36*(6), 893-906.

Pierpaoli, C., Barnett, A., Pajevic, S., Chen, R., Penix, L., Virta, A., & Basser, P. (2001). Water diffusion changes in Wallerian degeneration and their dependence on white matter architecture. *Neuroimage, 13*(6), 1174-1185. doi: DOI 10.1006/nimg.2001.0765

Rovaris, M., & Filippi, M. (2007). Diffusion tensor MRI in multiple sclerosis. [Review]. *Journal of Neuroimaging, 17 Suppl 1*, 27S-30S. doi: 10.1111/j.1552-6569.2007.00133.x

Rudrauf, D., Mehta, S., & Grabowski, T. J. (2008). Disconnection's renaissance takes shape: Formal incorporation in group-level lesion studies. [Validation Studies]. *Cortex, 44*(8), 1084-1096. doi: 10.1016/j.cortex.2008.05.005

Sisk, C. L., & Foster, D. L. (2004). The neural basis of puberty and adolescence. [Review]. *Nat Neurosci, 7*(10), 1040-1047. doi: 10.1038/nn1326

Smith, S. M., Jenkinson, M., Johansen-Berg, H., Rueckert, D., Nichols, T. E., Mackay, C. E., . . . Behrens, T. E. (2006). Tract-based spatial statistics: voxelwise analysis of multi-subject diffusion data. [Research Support, Non-U.S. Gov't]. *Neuroimage, 31*(4), 1487-1505. doi: 10.1016/j.neuroimage.2006.02.024

Somerville, L. H., Jones, R. M., & Casey, B. J. (2010). A time of change: behavioral and neural correlates of adolescent sensitivity to appetitive and aversive environmental cues. [Research Support, N.I.H., Extramural Research Support, Non-U.S. Gov't Review]. *Brain Cogn, 72*(1), 124-133. doi: 10.1016/j.bandc.2009.07.003

Schmahmann, J. D., Pandya, D. N., Wang, R., Dai, G., D'Arceuil, H. E., de Crespigny, A. J., & Wedeen, V. J. (2007). Association fibre pathways of the brain: parallel observations from diffusion spectrum imaging and autoradiography. *Brain, 130*, 630-653. doi: Doi 10.1093/Brain/Awl359

Sen, P. N., & Basser, P. J. (2005). A model for diffusion in white matter in the brain. *Biophys J, 89*(5), 2927-2938. doi: 10.1529/biophysj.105.063016

Sexton, C. E., Mackay, C. E., & Ebmeier, K. P. (2009). A systematic review of diffusion tensor imaging studies in affective disorders. [Research Support, Non-U.S. Gov't Review]. *Biol Psychiatry, 66*(9), 814-823. doi: 10.1016/j.biopsych.2009.05.024

Shu, N., Wang, Z., Qi, Z., Li, K., & He, Y. (2011). Multiple diffusion indices reveals white matter degeneration in Alzheimer's disease and mild cognitive impairment: a tract-based spatial statistics study. [Research Support, Non-U.S. Gov't]. *J Alzheimers Dis, 26 Suppl 3*, 275-285. doi: 10.3233/JAD-2011-0024

Smith, S. M., Jenkinson, M., Johansen-Berg, H., Rueckert, D., Nichols, T. E., Mackay, C. E., . . . Behrens, T. E. (2006). Tract-based spatial statistics: voxelwise analysis of multi-subject diffusion data. [Research Support, Non-U.S. Gov't]. *Neuroimage, 31*(4), 1487-1505. doi: 10.1016/j.neuroimage.2006.02.024

Stahl, R., Dietrich, O., Teipel, S. J., Hampel, H., Reiser, M. F., & Schoenberg, S. O. (2007). White matter damage in Alzheimer disease and mild cognitive impairment: assessment with diffusion-tensor MR imaging and parallel imaging techniques. *Radiology, 243*(2), 483-492. doi: 10.1148/radiol.2432051714

Stoub, T. R., DeToledo-Morrell, L., Stebbins, G. T., Leurgans, S., Bennett, D. A., & Shah, R. C. (2006). Hippocampal disconnection contributes to memory dysfunction in individuals at risk for Alzheimer's disease. *Proc Natl Acad Sci U S A, 103*(26), 10041-10045. doi: DOI 10.1073/pnas.0603414103

Stricker, N. H., Schweinsburg, B. C., Delano-Wood, L., Wierenga, C. E., Bangen, K. J., Haaland, K. Y., . . . Bondi, M. W. (2009). Decreased white matter integrity in late-myelinating fiber pathways in Alzheimer's disease supports retrogenesis. *Neuroimage, 45*(1), 10-16. doi: DOI 10.1016/j.neuroimage.2008.11.027

Sun, S. W., Liang, H. F., Cross, A. H., & Song, S. K. (2008). Evolving Wallerian degeneration after transient retinal ischemia in mice characterized by diffusion tensor imaging.

[Research Support, N.I.H., Extramural Research Support, Non-U.S. Gov't]. *Neuroimage, 40*(1), 1-10. doi: 10.1016/j.neuroimage.2007.11.049

Takahashi, S., Yonezawa, H., Takahashi, J., Kudo, M., Inoue, T., & Tohgi, H. (2002). Selective reduction of diffusion anisotropy in white matter of Alzheimer disease brains measured by 3.0 Tesla magnetic resonance imaging. [Comparative Study Research Support, Non-U.S. Gov't]. *Neurosci Lett, 332*(1), 45-48.

Takei, K., Yamasue, H., Abe, O., Yamada, H., Inoue, H., Suga, M., . . . Kasai, K. (2008). Disrupted integrity of the fornix is associated with impaired memory organization in schizophrenia. *Schizophrenia Research, 103*(1-3), 52-61. doi: DOI 10.1016/j.schres.2008.03.008

Teicher, M. H., Tomoda, A., & Andersen, S. L. (2006). Neurobiological consequences of early stress and childhood maltreatment: are results from human and animal studies comparable? [Research Support, N.I.H., Extramural Research Support, Non-U.S. Gov't Review]. *Ann N Y Acad Sci, 1071*, 313-323. doi: 10.1196/annals.1364.024

Teipel, S. J., Stahl, R., Dietrich, O., Schoenberg, S. O., Perneczky, R., Bokde, A. L. W., . . . Hampel, H. (2007). Multivariate network analysis of fiber tract integrity in Alzheimer's disease. *Neuroimage, 34*(3), 985-995. doi: DOI 10.1016/j.neuroimage.2006.07.047

Thompson, P. M., Hayashi, K. M., de Zubicaray, G., Janke, A. L., Rose, S. E., Semple, J., . . . Toga, A. W. (2003). Dynamics of gray matter loss in Alzheimer's disease. [Clinical Trial Controlled Clinical Trial Research Support, Non-U.S. Gov't Research Support, U.S. Gov't, P.H.S.]. *J Neurosci, 23*(3), 994-1005.

Versace, A., Almeida, J. R., Hassel, S., Walsh, N. D., Novelli, M., Klein, C. R., . . . Phillips, M. L. (2008). Elevated left and reduced right orbitomedial prefrontal fractional anisotropy in adults with bipolar disorder revealed by tract-based spatial statistics. [Research Support, N.I.H., Extramural Research Support, Non-U.S. Gov't]. *Arch Gen Psychiatry, 65*(9), 1041-1052. doi: 10.1001/archpsyc.65.9.1041

Van der Werf, Y. D., Jolles, J., Witter, M. P., & Uylings, H. B. (2003). Contributions of thalamic nuclei to declarative memory functioning. [Research Support, Non-U.S. Gov't Review]. *Cortex, 39*(4-5), 1047-1062.

Vargas, M. E., & Barres, B. A. (2007). Why is Wallerian degeneration in the CNS so slow? *Annual Review of Neuroscience, 30*, 153-179. doi: DOI 10.1146/annurev.neuro.30.051606.094354

Villain, N., Desgranges, B., Viader, F., de la Sayette, V., Mezenge, F., Landeau, B., . . . Chetelat, G. (2008). Relationships between hippocampal atrophy, white matter disruption, and gray matter hypometabolism in Alzheimer's disease. *Journal of Neuroscience, 28*(24), 6174-6181. doi: Doi 10.1523/Jneurosci.1392-08.2008

Vincent, J. L., Snyder, A. Z., Fox, M. D., Shannon, B. J., Andrews, J. R., Raichle, M. E., & Buckner, R. L. (2006). Coherent spontaneous activity identifies a hippocampal-parietal memory network. [Research Support, N.I.H., Extramural Research Support, Non-U.S. Gov't Research Support, U.S. Gov't, Non-P.H.S.]. *J Neurophysiol, 96*(6), 3517-3531. doi: 10.1152/jn.00048.2006

Wahlstrom, D., White, T., & Luciana, M. (2010). Neurobehavioral evidence for changes in dopamine system activity during adolescence. [Research Support, N.I.H., Extramural Research Support, Non-U.S. Gov't Review]. *Neurosci Biobehav Rev, 34*(5), 631-648. doi: 10.1016/j.neubiorev.2009.12.007

Wakana, S., Jiang, H., Nagae-Poetscher, L. M., van Zijl, P. C., & Mori, S. (2004). Fiber tract-based atlas of human white matter anatomy. [Research Support, U.S. Gov't, P.H.S.]. *Radiology, 230*(1), 77-87. doi: 10.1148/radiol.2301021640

Wang, Y., West, J. D., Flashman, L. A., Wishart, H. A., Santulli, R. B., Rabin, L. A., . . . Saykin, A. J. (2012). Selective changes in white matter integrity in MCI and older adults with cognitive complaints. *Biochim Biophys Acta, 1822*(3), 423-430. doi: 10.1016/j.bbadis.2011.08.002

Woods, R. P., Grafton, S. T., Holmes, C. J., Cherry, S. R., & Mazziotta, J. C. (1998). Automated image registration: I. General methods and intrasubject, intramodality validation. [Research Support, Non-U.S. Gov't Research Support, U.S. Gov't, Non-P.H.S. Research Support, U.S. Gov't, P.H.S.]. *J Comput Assist Tomogr, 22*(1), 139-152.

Xie, S., Xiao, J. X., Gong, G. L., Zang, Y. F., Wang, Y. H., Wu, H. K., & Jiang, X. X. (2006). Voxel-based detection of white matter abnormalities in mild Alzheimer disease. [Clinical Trial]. *Neurology, 66*(12), 1845-1849. doi: 10.1212/01.wnl.0000219625.77625.aa

Zhang, Y., Schuff, N., Jahng, G. H., Bayne, W., Mori, S., Schad, L., . . . Weiner, M. W. (2007). Diffusion tensor imaging of cingulum fibers in mild cognitive impairment and Alzheimer disease. [Comparative Study Research Support, N.I.H., Extramural Research Support, U.S. Gov't, Non-P.H.S.]. *Neurology, 68*(1), 13-19. doi: 10.1212/01.wnl.0000250326.77323.01

Zhuang, L., Wen, W., Zhu, W. L., Trollor, J., Kochan, N., Crawford, J., . . . Sachdev, P. (2010). White matter integrity in mild cognitive impairment: A tract-based spatial statistics study. *Neuroimage, 53*(1), 16-25. doi: DOI 10.1016/j.neuroimage.2010.05.068

BIOGRAPHICAL INFORMATION

Tejasvi Gundapuneedi completed her Bachelor of Engineering in Electronics and Communications from Jawaharlal Nehru Technological University (JNTU), Hyderabad, India in April 2006. Following graduation she pursued career as a software engineer for two years. Following her interest in the field of medical imaging she started her graduate studies in the Joint Program in Biomedical Engineering at the University of Texas at Arlington and University of Texas Southwestern Medical Center at Dallas in spring 2010. She joined the lab of Dr.Hao Huang at AIRC in spring 2011. From then she is involved in the research of Diffusion Tensor Imaging and its clinical applications.